

Light scattering by polydispersions of randomly oriented spheroids with sizes comparable to wavelengths of observation

Michael I. Mishchenko and Larry D. Travis

We report the results of an extensive study of the scattering of light by size and size–shape distributions of randomly oriented prolate and oblate spheroids with the index of refraction $1.5 + 0.02i$ typical of some mineral terrestrial aerosols. The scattering calculations have been carried out with Waterman's *T*-matrix approach, as developed recently by Mishchenko [J. Opt. Soc. Am. A **8**, 871 (1991); Appl. Opt. **32**, 4562 (1993)]. Our main interest is in light scattering by polydisperse models of nonspherical particles because averaging over sizes provides more realistic modeling of natural ensembles of scattering particles and washes out the interference structure and ripple typical of monodisperse scattering patterns, thus enabling us to derive meaningful conclusions about the effects of particle nonsphericity on light scattering. Following Hansen and Travis [Space Sci. Rev. **16**, 527 (1974)], we show that scattering properties of most physically plausible size distributions of randomly oriented nonspherical particles depend primarily on the effective equivalent-sphere radius and effective variance of the distribution, the actual shape of the distribution having a minor influence. To minimize the computational burden, we have adopted a computationally convenient power law distribution of particle equivalent-sphere radii $n(r) \propto r^{-3}$, $r_1 \leq r \leq r_2$. The effective variance of the size distribution is fixed at 0.1, and the effective size parameter continuously varies from 0 to 15. We present results of computer calculations for 24 prolate and oblate spheroidal shapes with aspect ratios from 1.1 to 2.2. The elements of the scattering matrix for the whole range of size parameters and scattering angles are displayed in the form of contour plots. Computational results are compared with analogous calculations for surface-equivalent spheres, and the effects of particle shape on light scattering are discussed in detail.

Key words: Light scattering, nonspherical particles, aerosols, remote sensing.

1. Introduction

Quantitative studies of the effects of atmospheric aerosols on the propagation of light through the atmosphere require accurate information regarding scattering properties of the aerosol particles. A substantial fraction of aerosols in terrestrial and planetary atmospheres can be composed of solid materials, thus implying nonspherical particle shapes, and we must expect that the particles are distributed over

sizes, shapes, and orientations. Also, the aerosol particles often have sizes comparable to the wavelength of light, thus precluding the use of the Rayleigh or geometric optics approximations. As a consequence the calculation of light scattering by atmospheric aerosols is demanding and requires the fastest possible numerical techniques for practical applications. Of course the same problem of computing light-scattering properties of polydisperse nonspherical particles can be important in many other areas, such as oceanography, biology, astrophysics, colloidal chemistry, and particle sizing.

Because of computational difficulties, the literature in which light-scattering calculations for polydisperse ensembles of nonspherical particles are reported and discussed is extremely scarce, and all previous studies of polydisperse nonspherical scattering were based on computations for only a few tens or a few hundreds of individual nonspherical particles.^{1–8} Furthermore, almost all computations of polydisperse nonspherical

M. I. Mishchenko is with the NASA Goddard Institute for Space Studies, Hughes STX Corporation, 2880 Broadway, New York, New York 10025. L. D. Travis is with the NASA Goddard Institute for Space Studies, 2880 Broadway, New York, New York 10025.

Received 18 November 1993; revised manuscript received 20 April 1994.

0003-6935/94/307206-20\$06.00/0.

© 1994 Optical Society of America.

scattering were restricted to photometric quantities such as the total optical cross sections, the single-scattering albedo, and the (1, 1) element of the scattering matrix, i.e., the phase function,¹⁻⁴ whereas only limited numerical data are available for other elements of the scattering matrix.⁵⁻⁸

Recently an efficient method for rigorously calculating the scattering of light by randomly oriented, rotationally symmetric particles of a size comparable to the wavelength of radiation has been developed, as described by Mishchenko.⁹ This method uses the analyticity of Waterman's *T*-matrix approach¹⁰⁻¹² and provides analytical rather than numerical averaging of light-scattering characteristics over particle orientations. In other words the orientational averaging step in actual computer calculations is essentially avoided, thus making the method numerically simple and fast. The method has been substantially improved by developing an efficient automatic convergence procedure that takes into account particular features of the *T*-matrix approach, as applied to randomly oriented particles, thereby substantially reducing computer time and storage requirements.¹³ Because numerical convergence is checked automatically, this procedure is especially suitable for computations of light scattering by size-shape distributions of nonspherical particles. Furthermore, recently Mishchenko and Travis¹⁴ have demonstrated that calculating the *T*-matrix with extended-precision instead of double-precision floating-point variables enables one to suppress the numerical instability of *T*-matrix computations. As a result the maximum particle size parameter for which *T*-matrix computations converge increases by a factor exceeding 2.

In this paper we apply Mishchenko's method to extensive study of light scattering by size and size-shape distributions of randomly oriented prolate and oblate spheroids with sizes comparable to the wavelength of light. Specifically, we examine how the optical cross sections, albedo for single scattering, asymmetry parameter of the phase function, and elements of the scattering matrix depend on the effective particle size and particle nonsphericity. We emphasize here that our main interest is in light scattering by polydisperse models of nonspherical particles because (1) averaging over sizes provides more realistic modeling of natural ensembles of scattering particles and (2) comparing scattering properties of particles of a single size is often meaningless because of the complicated interference structure and high-frequency ripple of scattering patterns.^{2,15-19} Averaging over particle sizes washes out the interference structure and ripple and, thus, permits meaningful comparisons of light-scattering properties of particles with different shapes and sizes.

Our specific goal here is not to study a limited selection of particle sizes, as was usually done in previous investigations of nonspherical scattering, but rather to present and analyze calculations for the continuous range of effective size parameters from zero to some maximum value to provide a general

picture of polydisperse spheroidal light scattering. In displaying the computational data we use contour plots of the elements of the scattering matrix as functions of scattering angle and size parameter. In conjunction with the smoothing effect of averaging over a size distribution, this provides an efficient display of a rather large amount of information and permits us to make meaningful and rather general conclusions about the effects of particle nonsphericity on light scattering.

We had several reasons to select spheroidal shapes for this investigation. First, the shape of a spheroid has the advantage of being described by only one shape parameter, specifically, the aspect ratio. By varying this single parameter, one can model a wide variety of nonspherical shapes ranging from spheres to needles and plates. Second, spheroids are rotationally symmetric particles and, therefore, are especially suitable for efficient *T*-matrix computations. Third, unlike cylinders (which are also described by only one shape parameter and can be treated by the *T*-matrix method^{7,20}), the surface of spheroids is smooth, thus permitting convergent *T*-matrix computations for larger particle sizes and aspect ratios. Fourth, before we attempt to model more complicated shapes, it seems useful to understand light-scattering properties of simple nonspherical particles in detail. Indeed, some features of nonspherical scattering may be the consequence of just the fact of particle nonsphericity or may depend on a rather general characteristic of particle shape such as, e.g., the ratio of the largest to the smallest particle dimensions. On the other hand, with a limited volume of computational data for a few arbitrarily selected nonspherical particles, one might be prone to erroneous interpretation of peculiarities of the scattering pattern as specific to one particular shape or, on the contrary, one might groundlessly consider these peculiarities a general property of nonspherical scattering. In this regard, an extensive survey of spheroidal scattering seems to be rather useful, at least in application to convex scatterers.

In Section 2 we introduce the definitions necessary to describe the shape of spheroidal particles and their distribution over sizes and briefly recapitulate basic quantities relevant to the scattering of light by randomly oriented rotationally symmetric particles. Then we present results of extensive calculations of light scattering by polydispersions of surface-equivalent spheres and randomly oriented prolate and oblate spheroids with aspect ratios from 1.1 to 2.2. Our observations and conclusions regarding the effects of particle shape on the optical cross sections, single-scattering albedo, asymmetry parameter of the phase function, and elements of the scattering matrix based on these calculations are discussed in Section 3. In Section 4 the main results of the paper are summarized. Some preliminary results of this study have been previously reported,²¹ and a comprehensive study of polydisperse nonspherical linear polarization is presented in a separate paper.¹⁹

2. Calculations

The shape of a spheroid in the spherical coordinate system is governed by the equation

$$r(\vartheta, \phi) = a \left[\sin^2 \vartheta + \frac{a^2}{b^2} \cos^2 \vartheta \right]^{-1/2}, \quad (1)$$

where ϑ is the zenith angle, ϕ is the azimuth angle, b is the rotational (vertical) semiaxis, and a is the horizontal semiaxis. To specify the shape and size of a prolate or an oblate spheroid, we use the couple (ϵ, r) , where $\epsilon \geq 1$ is the aspect ratio defined as $\epsilon = b/a$ for prolate spheroids and as $\epsilon = a/b$ for oblate spheroids, and r is the radius of the equal-surface-area sphere (or, equivalently,²² the radius of the sphere that has the cross-sectional area equal to the averaged projected area of randomly oriented spheroids) given by

$$r = \frac{1}{2} \left[2a^2 + 2ab \frac{\arcsin e}{e} \right]^{1/2} \quad (2)$$

for prolate spheroids and by

$$r = \frac{1}{2} \left[2a^2 + \frac{b^2}{e} \ln \left(\frac{1+e}{1-e} \right) \right]^{1/2} \quad (3)$$

for oblate spheroids, where

$$e = \frac{(\epsilon^2 - 1)^{1/2}}{\epsilon}. \quad (4)$$

The single scattering of light by a small-volume element consisting of randomly oriented, rotationally symmetric, independently scattering particles is completely specified by the cross sections for scattering C_{sca} and extinction C_{ext} and the elements of the normalized scattering matrix \mathbf{F} .¹⁵⁻¹⁷ In the standard $\{I, Q, U, V\}$ representation of polarization, the scattering matrix has the form

$$\mathbf{F}(\Theta) = \begin{bmatrix} F_{11}(\Theta) & F_{12}(\Theta) & 0 & 0 \\ F_{12}(\Theta) & F_{22}(\Theta) & 0 & 0 \\ 0 & 0 & F_{33}(\Theta) & F_{34}(\Theta) \\ 0 & 0 & -F_{34}(\Theta) & F_{44}(\Theta) \end{bmatrix}, \quad (5)$$

where $\Theta \in [0, \pi]$ is the scattering angle and the $(1, 1)$ element (i.e., the phase function) satisfies the normalization condition

$$\frac{1}{4\pi} \int_{4\pi} d\Omega F_{11}(\Theta) = 1. \quad (6)$$

Additional important quantities describing light scattering are the absorption cross section $C_{\text{abs}} = C_{\text{ext}} - C_{\text{sca}}$, the single-scattering albedo $\varpi = C_{\text{sca}}/C_{\text{ext}}$, and the asymmetry parameter of the phase function (or mean cosine of the scattering angle), $g = \langle \cos \Theta \rangle$.¹⁵⁻¹⁷

To calculate the cross sections and the elements of the scattering matrix for a size distribution of randomly oriented, rotationally symmetric particles, we used the method described in detail in Refs. 9 and 13. In all our calculations, we used the value of the convergence parameter Δ [Eqs. (18) and (21) of Ref. 13] equal to 10^{-3} .

Hansen and Travis¹⁶ (see also Refs. 23 and 24) have shown that scattering properties of most physically plausible size distributions of spherical particles depend primarily on only two characteristics of the distribution, the effective radius r_{eff} and the effective variance ν_{eff} , the particular shape of the distribution being of secondary importance. The effective radius is defined as the cross-sectional-area-weighted mean radius,

$$r_{\text{eff}} = \frac{1}{G} \int_0^\infty dr r \pi r^2 n(r), \quad (7)$$

where

$$G = \int_0^\infty dr \pi r^2 n(r) \quad (8)$$

is the average geometric cross-sectional area and $n(r)dr$ is the fraction of the particles with radii between r and $r + dr$. Note that

$$\int_0^\infty dr n(r) = 1. \quad (9)$$

Similarly, the width of the distribution is characterized by the dimensionless effective variance ν_{eff} defined as

$$\nu_{\text{eff}} = \frac{1}{Gr_{\text{eff}}^2} \int_0^\infty dr (r - r_{\text{eff}})^2 \pi r^2 n(r). \quad (10)$$

Thus the result of Hansen and Travis means that if different size distributions of spherical particles have the same values of the effective radius and effective variance, then their scattering properties are practically identical. To verify whether this result also applies to nonspherical particles, we computed the light-scattering properties of three size distributions of randomly oriented oblate spheroids, namely, power law, gamma, and log-normal distributions given by¹⁶

$$n(r) = \begin{cases} \frac{2r_1^2 r_2^2}{r_2^2 - r_1^2} r^{-3} & \text{for } r_1 \leq r \leq r_2, \\ 0 & \text{otherwise,} \end{cases} \quad (11)$$

$$n(r) = \text{constant } r^{(1-3\nu_{\text{eff}})/\nu_{\text{eff}}} \exp\left(-\frac{r}{r_{\text{eff}}\nu_{\text{eff}}}\right), \quad (12)$$

$$n(r) = \frac{1}{(2\pi)^{1/2}\sigma_g} \frac{1}{r} \exp\left[-\frac{(\ln r - \ln r_g)^2}{2\sigma_g^2}\right], \quad (13)$$

respectively, where r is now the radius of the equal-surface-area sphere. The aspect ratio of the spheroids is 1.7, and their refractive index is $1.5 + 0.02i$. Note that Eq. (12) for the gamma distribution uses the effective radius and the effective variance as formal parameters, and the formal parameters r_1 , r_2 , σ_g , and r_g for the power law and log-normal distributions correspond to r_{eff} and ν_{eff} values according to the following relations¹⁶:

$$r_{\text{eff}} = \frac{r_2 - r_1}{\ln(r_2/r_1)}, \quad (14)$$

$$\nu_{\text{eff}} = \frac{r_2 + r_1}{2(r_2 - r_1)} \ln(r_2/r_1) - 1, \quad (15)$$

$$r_{\text{eff}} = r_g \exp(5\sigma_g^2/2), \quad (16)$$

$$\nu_{\text{eff}} = \exp(\sigma_g^2) - 1. \quad (17)$$

The values of the formal parameters for all the three size distributions were chosen such that they had the same effective radius $r_{\text{eff}} = 1.5 \mu\text{m}$ and effective variance $\nu_{\text{eff}} = 0.1$ (Fig. 1). Although the range of particle radii for the gamma and log-normal distributions is, theoretically, infinite, in practical computer calculations one must truncate the range at a maximum radius chosen such that scattering properties of polydisperse particles are computed within a given accuracy. Specifically, the ranges of the radii in our calculations were $[0, 4] \mu\text{m}$ and $[0, 4.5] \mu\text{m}$ for the gamma and the log-normal distributions, respectively, which guaranteed the relative accuracy of computation of the extinction and scattering cross sections better than 10^{-4} . For comparison, the range of particle radii $[r_1, r_2]$ for the power law distribution was $[0.8202, 2.4799] \mu\text{m}$. The number of Gaussian division points used in numerical averaging over particle radii was also chosen to provide the specified accuracy and was 70 for the power law distribution, 100 for the gamma distribution, and 110 for the log-normal distribution.

The results of our computations at a wavelength

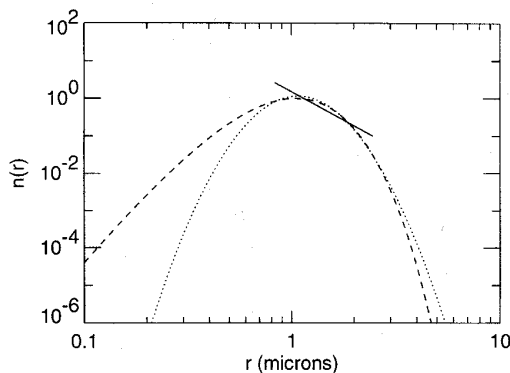


Fig. 1. Power law (—), gamma (---), and log-normal (.....) size distributions having the same effective radius $r_{\text{eff}} = 1.5 \mu\text{m}$ and effective variance $\nu_{\text{eff}} = 0.1$.

Table 1. Optical Cross Sections, Single-Scattering Albedo, and Asymmetry Parameter of the Phase Function for Power Law, Gamma, and Log-Normal Distributions of Equivalent-Sphere Radii for Randomly Oriented Oblate Spheroids with Aspect Ratio 1.7^a

Size Distribution	C_{ext}^b	C_{sca}^b	C_{abs}^b	ω	$\langle \cos \Theta \rangle$
Power law	12.19	8.18	4.01	0.671	0.822
Gamma	11.94	8.06	3.88	0.675	0.825
Log-normal	12.42	8.36	4.06	0.673	0.825

^aAll three distributions have the same effective radius $r_{\text{eff}} = 1.5 \mu\text{m}$ and effective variance $\nu_{\text{eff}} = 0.1$. The refractive index of the spheroids is $1.5 + 0.02i$, and the wavelength is $0.6283 \mu\text{m}$.

^bIn square micrometers.

$\lambda = 0.6283 \mu\text{m}$ are shown in Table 1 and Fig. 2. We do not display the elements of the scattering matrix for the gamma distribution because in most cases the corresponding curves were hardly distinguishable from those for the log-normal distribution. One can see that despite the quite different shapes of the size distributions (Fig. 1), the computed light-scattering characteristics are in excellent quantitative agreement. This comparison confirms and extends to randomly oriented spheroidal particles the conclusion of Hansen and Travis that, irrespective of the particular shape of a size distribution, its scattering properties are completely specified by only two parameters, namely, effective radius and effective variance.

From the perspective of efficiency, however, we note that the CPU times on an IBM RISC model 37T workstation for the three optically equivalent size distributions were dramatically different: 28 min for the power law distribution, 6 h for the gamma distribution, and 14 h for the log-normal distribution. These big differences are explained by the fact that the CPU time for T -matrix computations increases as the third or even fourth power of the particle size parameter and that convergent computations for size parameters above some critical value can only be performed with extended-precision arithmetic.¹⁴ In view of similarity of the optical scattering characteristics corresponding to different distributions with equivalent r_{eff} and ν_{eff} , the substantially greater efficiency for the power law distribution makes an obvious case for its use, especially for a survey intended to cover a broad range of r_{eff} values and aspect ratios. Although at present the T -matrix method is by far the fastest numerical tool for rigorously computing light scattering by randomly oriented nonspherical particles,¹⁹ even with this method the CPU time consumed can still be significant, especially for big or highly aspherical scatterers. Therefore, to minimize the computational burden, we have adopted the power law distribution for all further calculations reported in this paper. However, as the above comparison illustrates, it is reasonable to presume that all our computations and conclusions remain valid for any other distribution, including gamma and log-normal distributions having the same r_{eff} and ν_{eff} .

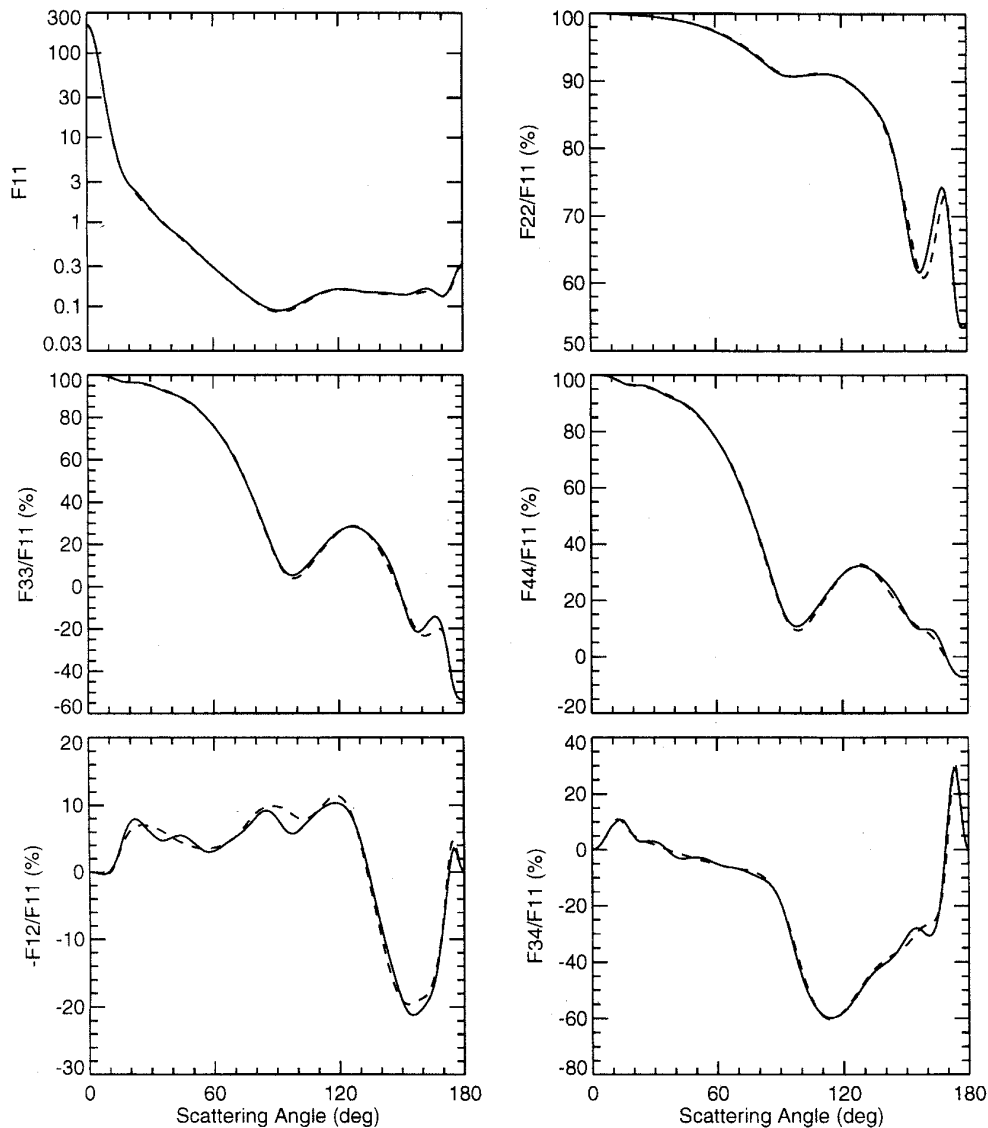


Fig. 2. Elements of the scattering matrix for power law (—) and log-normal (---) distributions of equivalent-sphere radii for randomly oriented oblate spheroids with aspect ratio 1.7. For both distributions, the effective radius is $r_{\text{eff}} = 1.5 \mu\text{m}$ and the effective variance is $v_{\text{eff}} = 0.1$. The refractive index of the spheroids is $1.5 + 0.02i$, and the wavelength is $0.6283 \mu\text{m}$.

Note that for a fixed v_{eff} , the minimum, r_1 , and maximum, r_2 , radii of the power law distribution are proportional to r_{eff} . Defining $q_1 = r_1/r_{\text{eff}}$ and $q_2 = r_2/r_{\text{eff}}$, we determine these proportionality factors by solving numerically the following system of two (non-linear) equations [cf. Eqs. (14) and (15)]:

$$\frac{(q_2 - q_1)}{\ln(q_2/q_1)} = 1, \quad (18)$$

$$q_2 + q_1 = 2(v_{\text{eff}} + 1). \quad (19)$$

The values of q_1 and q_2 for a selection of v_{eff} values are tabulated in Ref. 19.

We have performed calculations for 12 prolate and 12 oblate spheroidal shapes with aspect ratios 1.1 (0.1) 2.2. However, to keep this paper to a reasonable size, below we display only the results for prolate and oblate spheroids with aspect ratios 1.5 and 2.2. These particular aspect ratios have been chosen based on our study of polydisperse nonspherical polarization¹⁹ and are intended to represent moderately ($\epsilon = 1.5$) and strongly ($\epsilon = 2.2$) aspherical particles. In particular, although for particles with the aspect ratio $\epsilon = 1.5$ the pattern of linear polarization is already distinctly different from that for surface-equivalent spheres, it does not show yet the pronounced bridge of positive polarization at scattering

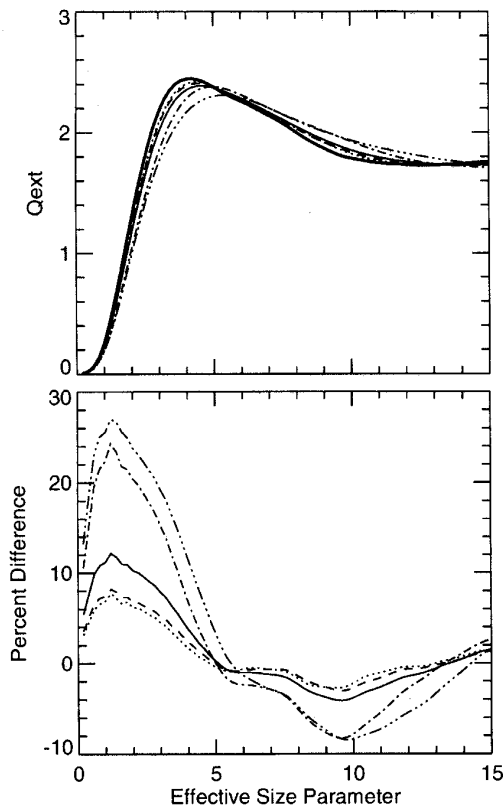


Fig. 3. Upper graph, efficiency factor for extinction Q_{ext} versus effective size parameter x_{eff} for surface-equivalent polydispersions of spheres (—), randomly oriented prolate spheroids with aspect ratios $\epsilon = 1.5$ (.....) and 2.2 (-·-·-·-), randomly oriented oblate spheroids with aspect ratios $\epsilon = 1.5$ (---) and $\epsilon = 2.2$ (- - - -), and an equiprobable mixture of 24 spheroidal shapes (—). Lower graph, corresponding percent spherical-non-spherical differences ϵ_{ext} defined by Eq. (21).

angles near 120° that appears for particles with a larger degree of nonsphericity and is definitely present for particles with $\epsilon = 2.2$. We also display results for computations for the simplest, equiprobable mixture of all the 24 spheroidal shapes. Thus we assume that $J = 24$ and $p_j = 1/24$ in equations 10–13 of Ref. 13.

Throughout this paper we use a constant effective variance $\nu_{\text{eff}} = 0.1$, corresponding to a moderately wide size distribution, and a refractive index $N = 1.5 + 0.02i$. This index of refraction is typical of some terrestrial aerosols at visible wavelengths²⁵ and was used by Wiscombe and Mugnai^{1–3,26} in their light-scattering computations for Chebyshev particles. Note that for $\nu_{\text{eff}} = 0.1$, $r_1 \approx 0.54677 r_{\text{eff}}$ and $r_2 \approx 1.65324 r_{\text{eff}}$.

The results of our numerical calculations are presented in Figs. 3–13, below. Figures 3, 4, 5, 6, and 7 show the efficiency factors for extinction (Q_{ext}), scattering (Q_{sca}), and absorption (Q_{abs}), the albedo for single scattering (ω), and the asymmetry parameter of the phase function, $\langle \cos \Theta \rangle$, respectively, as functions of the effective size parameter $x_{\text{eff}} = 2\pi r_{\text{eff}}/\lambda$, with the

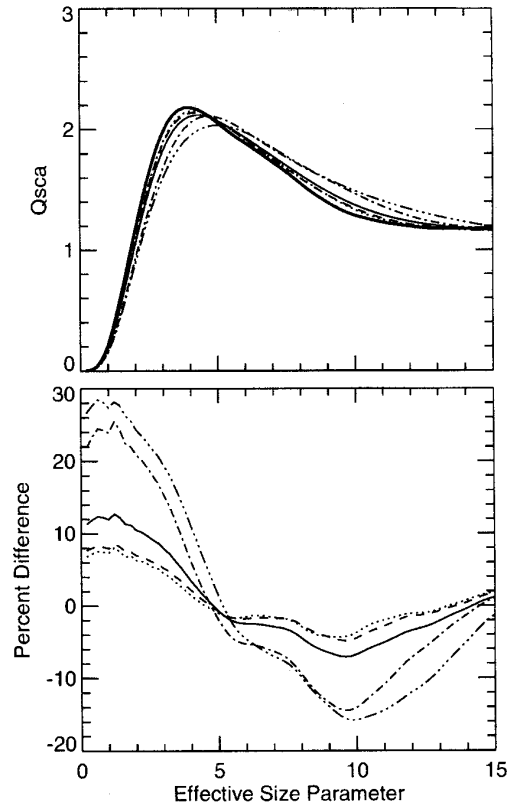


Fig. 4. Upper graph, efficiency factor for scattering Q_{sca} versus effective size parameter x_{eff} for surface-equivalent polydispersions of spheres (—), randomly oriented prolate spheroids with aspect ratios $\epsilon = 1.5$ (.....) and 2.2 (-·-·-·-), randomly oriented oblate spheroids with aspect ratios $\epsilon = 1.5$ (---) and $\epsilon = 2.2$ (- - - -), and an equiprobable mixture of 24 spheroidal shapes (—). Lower graph, corresponding percent spherical-non-spherical differences.

wavelength set at $\lambda = 2\pi/10 \approx 0.6283 \mu\text{m}$. The efficiency factors are defined as

$$Q_{\text{ext}} = \frac{C_{\text{ext}}}{\pi r_{\text{eff}}^2}, \quad Q_{\text{sca}} = \frac{C_{\text{sca}}}{\pi r_{\text{eff}}^2}, \quad Q_{\text{abs}} = \frac{C_{\text{abs}}}{\pi r_{\text{eff}}^2}. \quad (20)$$

In Figs. 3–7 the effective radius continuously varies from 0 to $1.5 \mu\text{m}$. Therefore the maximum effective size parameter is equal to 15, which, for size distributions with $\nu_{\text{eff}} = 0.1$, requires calculation for a maximum monodisperse equivalent-sphere size parameter equal to 24.8. Also, the lower panels in Figs. 3–7 show the corresponding percent spherical-non-spherical differences, defined as

$$\epsilon_{\text{ext}} = \frac{C_{\text{ext}}(\text{spherical}) - C_{\text{ext}}(\text{nonspherical})}{C_{\text{ext}}(\text{spherical})} \times 100\% \quad (21)$$

for the extinction cross section and analogously for C_{sca} , C_{abs} , ω , and $\langle \cos \Theta \rangle$.

Figures 9–13 are contour plots of the elements of

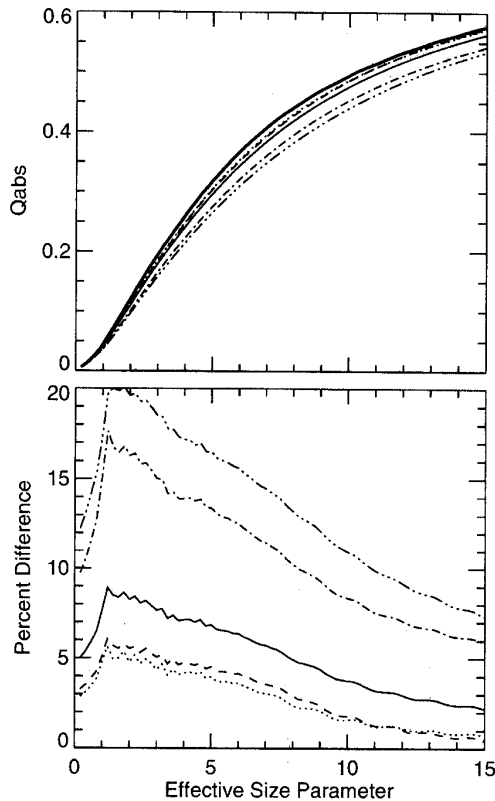


Fig. 5. Upper graph, efficiency factor for absorption Q_{abs} versus effective size parameter x_{eff} for surface-equivalent polydispersions of spheres (—), randomly oriented prolate spheroids with aspect ratios $\epsilon = 1.5$ (.....) and 2.2 (— · — · —), randomly oriented oblate spheroids with aspect ratios $\epsilon = 1.5$ (— · — · —) and $\epsilon = 2.2$ (— · — · —), and an equiprobable mixture of 24 spheroidal shapes (—). Lower graph, corresponding percent spherical-nonspherical differences.

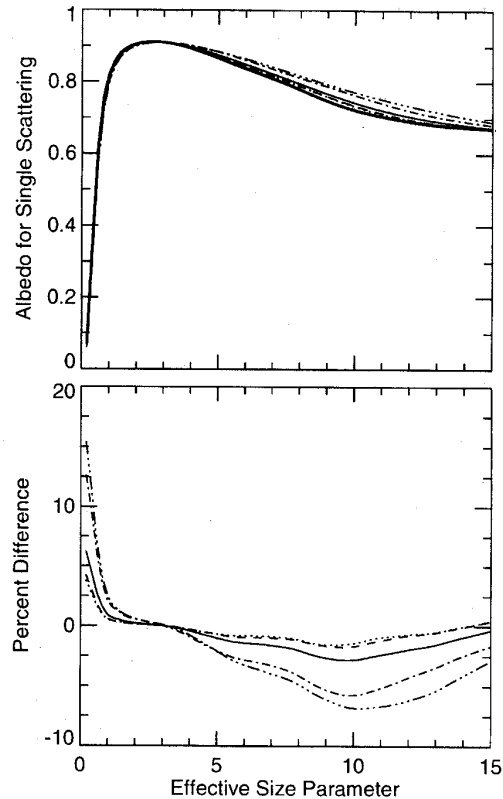


Fig. 6. Upper graph, single-scattering albedo α versus effective size parameter x_{eff} for surface-equivalent polydispersions of spheres (—), randomly oriented prolate spheroids with aspect ratios $\epsilon = 1.5$ (.....) and 2.2 (— · — · —), randomly oriented oblate spheroids with aspect ratios $\epsilon = 1.5$ (— · — · —) and $\epsilon = 2.2$ (— · — · —), and an equiprobable mixture of 24 spheroidal shapes (—). Lower graph, corresponding percent spherical-nonspherical differences.

the scattering matrix as functions of the scattering angle $0^\circ \leq \Theta \leq 180^\circ$ (horizontal axes) and the effective size parameter $0 \leq x_{eff} \leq 15$ (vertical axes). Note that for spheres

$$F_{22}(\Theta)/F_{11}(\Theta) \equiv 1, \quad (22)$$

$$F_{33}(\Theta)/F_{11}(\Theta) \equiv F_{44}(\Theta)/F_{11}(\Theta). \quad (23)$$

Figure 8 shows a contour plot of the normalized phase function for polydisperse spheres accompanied by contour plots of percent spherical-nonspherical differences in intensity for polydisperse spheroids, defined as

$$\epsilon_f(\Theta) = \frac{[F_{11}(\Theta)]_{spherical} - [F_{11}(\Theta)]_{nonspher}}{[F_{11}(\Theta)]_{spherical}} \times 100\%. \quad (24)$$

The computational data displayed in Figs. 3–13 represent calculations for over 80,000 individual nonspherical particles in random orientation and were

calculated in approximately 120 h of CPU time on an IBM RISC/6000 model 37T workstation.

3. Discussion

A. Optical Cross Sections, Single-Scattering Albedo, and Asymmetry Parameter of the Phase Function

The common feature of Figs. 3–7 is that spherical-nonspherical differences increase in absolute value as the aspect ratio increases and are similar for prolate and oblate spheroids of the same aspect ratio. Spherical extinction and scattering cross sections are larger than nonspherical cross sections for effective size parameters from 0 to roughly 5 but become smaller for x_{eff} from 5 to 13–15. Figure 5 shows that, for the specific refractive index, effective variance, and range of effective size parameters, spheres are stronger absorbers than surface-equivalent spheroids. Spherical single-scattering albedos are larger than nonspherical single-scattering albedos for x_{eff} from 0 to 3.5 and are smaller for larger particles.

It is well known (see, e.g., van de Hulst¹⁵ and Bohren and Huffman¹⁷) that for particles much

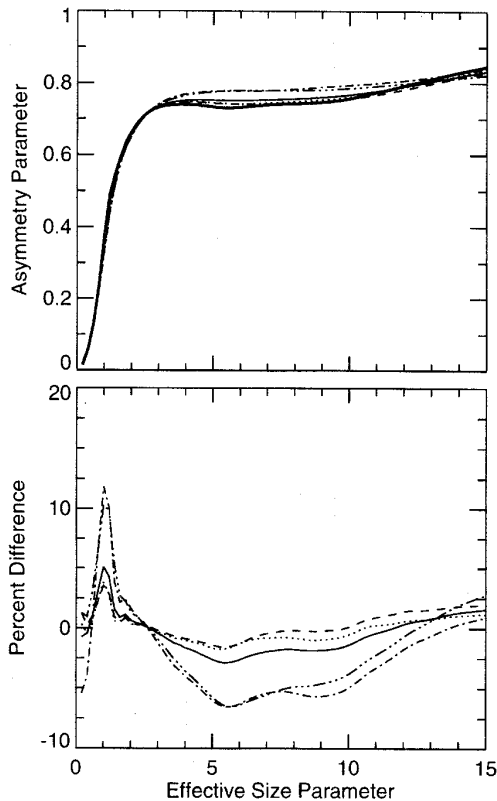


Fig. 7. Upper graph, asymmetry parameter of the phase function ($\cos \Theta$) versus effective size parameter x_{eff} for surface-equivalent polydispersions of spheres (—), randomly oriented prolate spheroids with aspect ratios $\epsilon = 1.5$ (.....) and 2.2 (— · — · —), randomly oriented oblate spheroids with aspect ratios $\epsilon = 1.5$ (— · — · —) and $\epsilon = 2.2$ (— · — · —), and an equiprobable mixture of 24 spheroidal shapes (— · — · —). Lower graph, corresponding percent spherical-nonspherical differences.

smaller than a wavelength, the extinction cross section is proportional to particle volume, not particle surface or cross-sectional area. Therefore large spherical-nonspherical differences seen in Figs. 3–6 for small particles are partly an artifact of using the equivalent-sphere radius rather than the equal-volume-sphere radius to specify the size of the spheroids. Indeed, we have found that analogous calculations for equal-volume particles reveal smaller spherical-nonspherical differences for the optical cross sections and the single-scattering albedo in the region of small size parameters ($x \leq 5$). However, spherical-nonspherical differences in extinction and scattering are smaller for surface-equivalent particles than for volume-equivalent particles for x_{eff} larger than roughly 5. We have also found that spherical-nonspherical differences in the asymmetry parameter of the phase function are essentially insensitive to whether surface-equivalent or volume-equivalent particles are compared. Therefore Fig. 7 demonstrates the limited applicability of the semiempirical theory of Pollack and Cuzzi,²⁷ which yields smaller asymmetry parameters for nonspherical particles than for

their equal-volume spherical counterparts with size parameters larger than approximately 5 (see also Ref. 28).

We have found that the integral photometric properties of the equiprobable mixture of particle shapes can be rather accurately represented by those of a single spheroidal shape. Specifically, for the whole range of effective size parameters from 0 to 15, the absolute percent difference between the equiprobable shape mixture and an oblate spheroid with the aspect ratio $\epsilon = 1.7$ is less than 1.6% in C_{ext} , less than 1.7% in C_{sca} , less than 1.3% in C_{abs} , less than 1.0% in the single-scattering albedo, and less than 2.0% in $\langle \cos \Theta \rangle$. This result is, of course, not unexpected, because these integral photometric quantities are relatively simple functions of particle size parameter and shape, are similar for prolate and oblate spheroids of the same aspect ratio, and change smoothly with increasing particle asphericity.

B. Phase Function (F_{11})

Our phase function calculations displayed in Fig. 8 show that for effective size parameters larger than roughly 4, the following five distinct regions exist, in order of increasing scattering angle:

- (1) sphere \approx nonsphere,
- (2) sphere $<$ nonsphere,
- (3) sphere $>$ nonsphere,
- (4) sphere $<$ nonsphere,
- (5) sphere $>$ nonsphere.

The first of these regions is the region of forward scattering ($\Theta = 0^\circ$ to 10 – 15°) that, in agreement with the conclusions of Wiscombe and Mugnai,² is the least-sensitive region to particle nonsphericity. Here the absolute value of spherical-nonspherical differences rarely exceeds 20%. In the calculations of Wiscombe and Mugnai² for moderately aspherical Chebyshev particles, nonspherical intensities in the forward-scattering region were always larger than spherical intensities. Our data show, however, that spheroidal particles with $x_{\text{eff}} \geq 10$ may scatter in this region as much as 10% less than surface-equivalent spheres [Fig. 8(c)].

In the second region, which, depending on effective size parameter, extends from $\Theta = 10$ – 20° to 30 – 45° , spheroids are stronger scatterers (in terms of the value of the normalized phase function) than surface-equivalent spheres, spherical-nonspherical differences increasing with increasing aspect ratio and reaching -45% . To our knowledge, the existence of this region was not mentioned before and demonstrates the restricted applicability of the conclusion of Wiscombe and Mugnai² that nonspheres scatter less than spheres in the 10 – 80° range of scattering angles. Note that Wiscombe and Mugnai made that conclusion on the basis of their computations for moderately aspherical Chebyshev particles. In laboratory measurements of light scattering, the range of the smallest scattering angles is usually inaccessible. Therefore comparisons of measured nonspherical

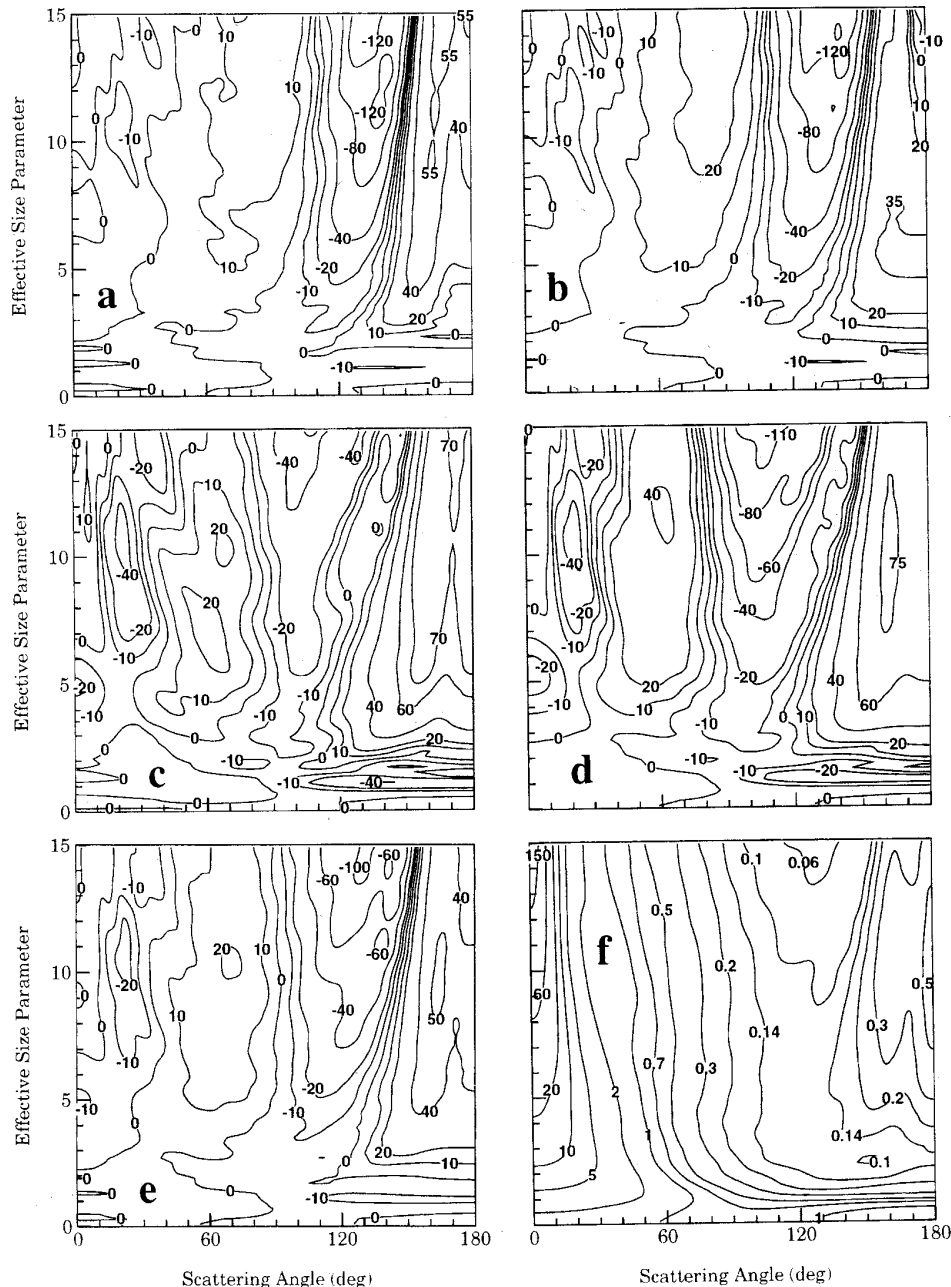


Fig. 8. Contour plots of ϵ_r [see Eq. (24)] as a function of scattering angle Θ and effective size parameter x_{eff} for surface-equivalent polydispersions of (a) prolate and (b) oblate spheroids with the aspect ratio $\epsilon = 1.5$, (c) prolate and (d) oblate spheroids with the aspect ratio $\epsilon = 2.2$, and (e) an equiprobable mixture of 24 spheroidal shapes. (f) contour plot of the normalized phase function for polydisperse spherical particles.

phase functions and phase functions computed theoretically for equivalent spheres are often made on the basis of equating the functions at a phase angle $\Theta = 10^\circ$ or 20° . Our results here show that such an approach is not necessarily an acceptable approximation and may lead to erroneous conclusions.

Region 3 extends from $\Theta = 40\text{--}50^\circ$ to $100\text{--}105^\circ$ for spheroids with the aspect ratio 1.5 and from $\Theta =$

$35\text{--}40^\circ$ to $75\text{--}80^\circ$ for spheroids with the aspect ratio 2.2. Once again the angle ranges are only nominal and change somewhat with particle size. Here spheres are stronger scatterers than nonspheres, with spherical-nonspherical differences increasing as the aspect ratio increases and exceeding +40% for oblate spheroids with the aspect ratio 2.2.

Region 4 is the region of side scattering and,

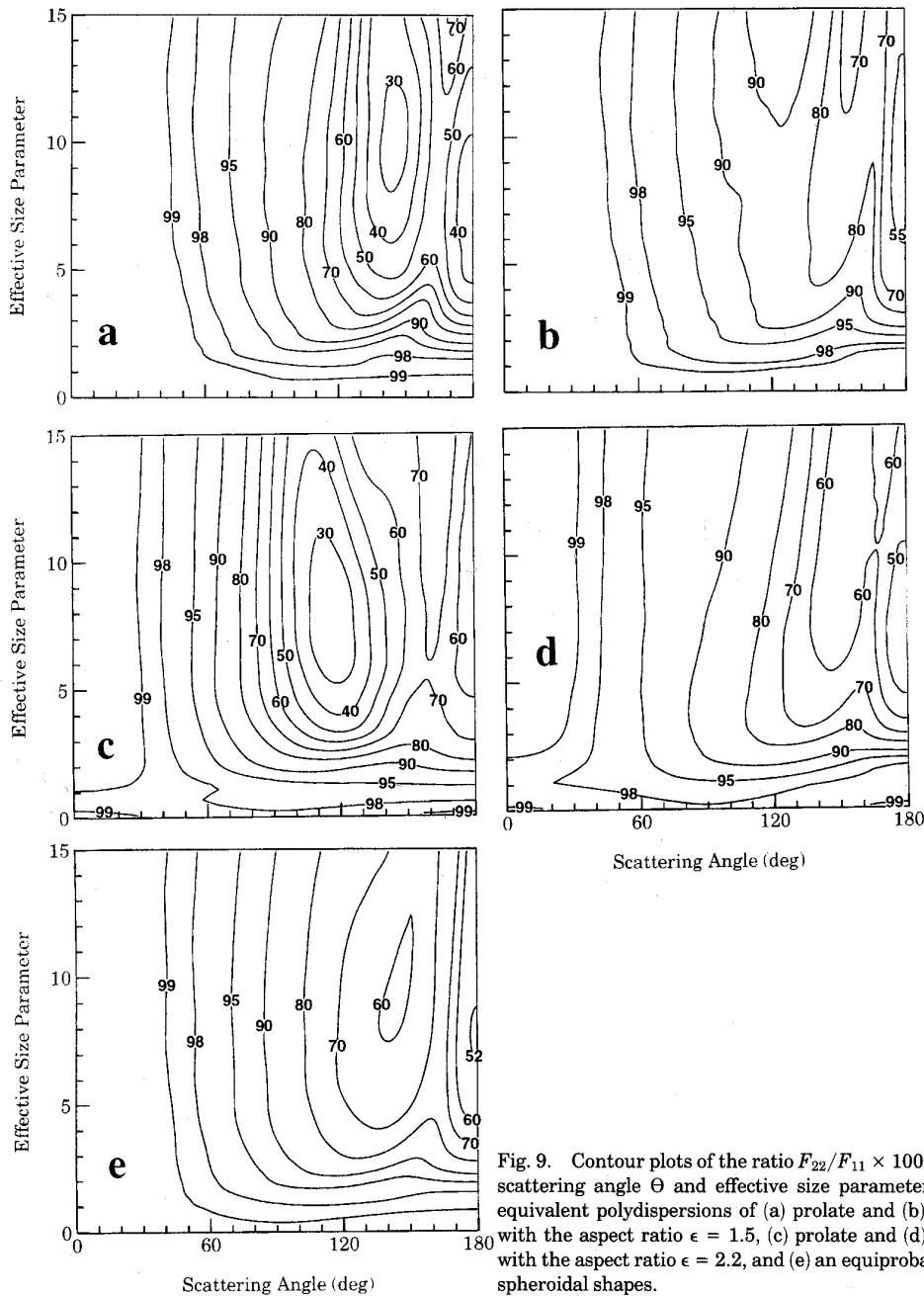


Fig. 9. Contour plots of the ratio $F_{22}/F_{11} \times 100\%$ as a function of scattering angle Θ and effective size parameter x_{eff} for surface-equivalent polydispersions of (a) prolate and (b) oblate spheroids with the aspect ratio $\epsilon = 1.5$, (c) prolate and (d) oblate spheroids with the aspect ratio $\epsilon = 2.2$, and (e) an equiprobable mixture of 24 spheroidal shapes.

depending on particle size, extends from $\Theta = 100\text{--}105^\circ$ to $135\text{--}150^\circ$ for spheroids with $\epsilon = 1.5$ and from $\Theta = 80\text{--}90^\circ$ to $120\text{--}145^\circ$ for spheroids with $\epsilon = 2.2$. In this region, nonspherical intensities are larger (up to a factor of 2.3) than spherical intensities (cf. Refs. 29 and 30). Interestingly, in this region, unlike all other regions, spherical-nonspherical differences are larger for the less aspherical spheroids with the aspect ratio 1.5.

The backscattering region (region 5) extends, depending on x_{eff} , from $\Theta = 140\text{--}160^\circ$ to 180° for spheroids with the aspect ratio 1.5 and from $\Theta =$

$125\text{--}155^\circ$ to 180° for spheroids with the aspect ratio 2.2. As was noted by Wiscombe and Mugnai,² this region, in which the glory occurs, is the most sensitive to the fact of sphericity. Here spherical-nonspherical differences are in most cases positive, increase with increasing aspect ratio, and can exceed +75%. In other words, the ratio of spherical to nonspherical phase functions in this region can exceed 4, which is in agreement with laboratory measurements by Perry *et al.*²⁹ for nearly cubically shaped NaCl particles. However, as was first pointed out by Wiscombe and Mugnai,² the backscattering peak, usually associated

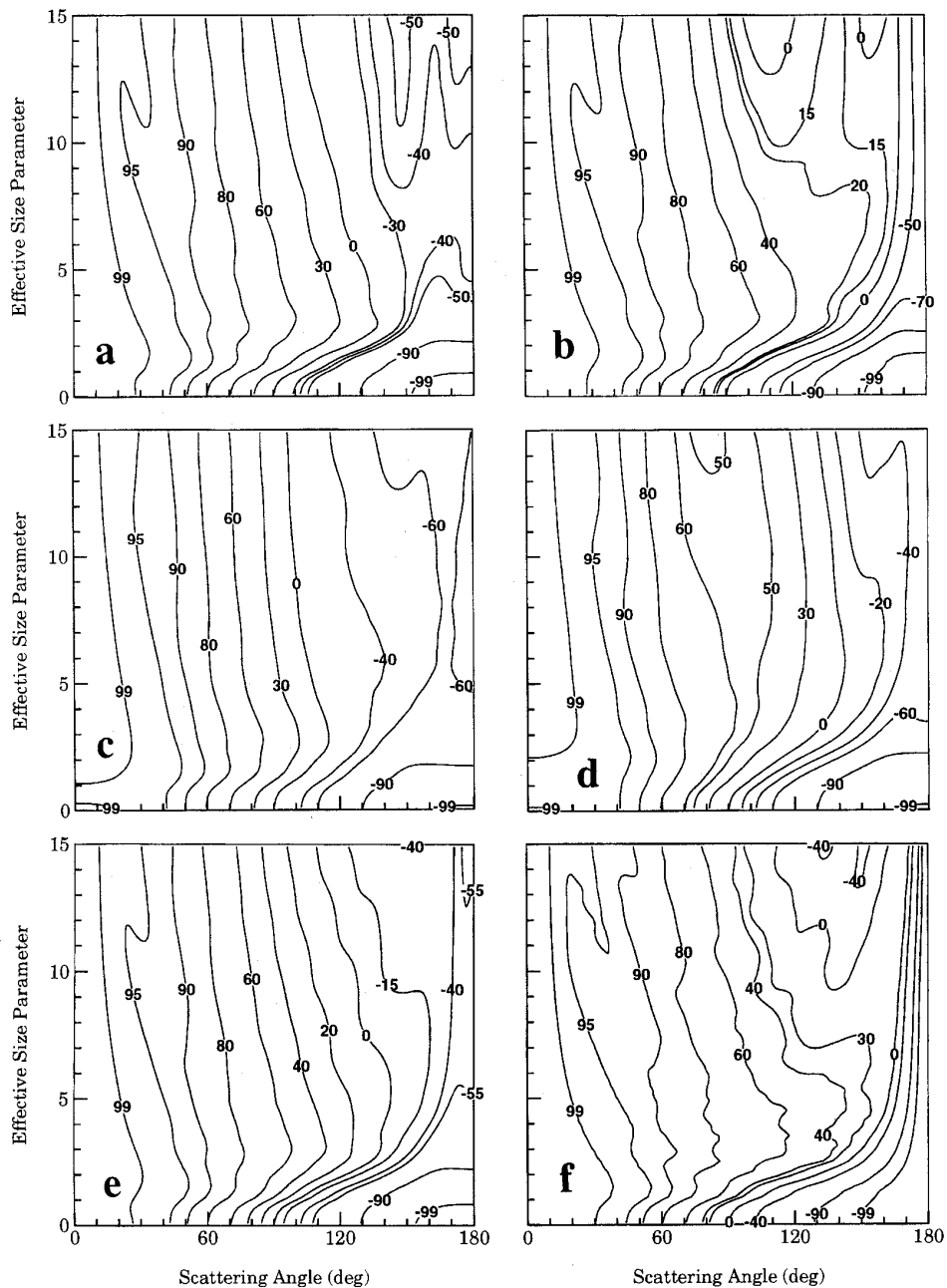


Fig. 10. Contour plots of the ratio $F_{33}/F_{11} \times 100\%$ as a function of scattering angle Θ and effective size parameter x_{eff} for surface-equivalent polydispersions of (a) prolate and (b) oblate spheroids with the aspect ratio $\epsilon = 1.5$, (c) prolate and (d) oblate spheroids with the aspect ratio $\epsilon = 2.2$, (e) an equiprobable mixture of 24 spheroidal shapes, and (f) spheres.

with the glory, survives as a rise of the backscattered intensity at $\Theta = 180^\circ$ relative to that at $\Theta = 170^\circ$. This modest backscattering peak is also seen in figure 7 of Ref. 4 and figures 2 and 3 of Ref. 13. Interestingly, in the backscattering region prolate-oblate differences are much smaller for particles with $\epsilon = 2.2$ than for less-irregular particles with $\epsilon = 1.5$. Although for prolate spheroids with the aspect ratio 1.5 the backscattering peak is substantially depressed,

for oblate spheroids with the same aspect ratio the spherical-nonspherical differences at backscattering angles are much smaller and even become negative at effective size parameters near 13–15, thus indicating that the oblate spheroids become stronger scatterers than surface-equivalent spheres (see also figures 2 and 3 of Ref. 13).

Unlike regions 2 and 3, which become practically indistinguishable below $x_{\text{eff}} = 4$, region 1 extends

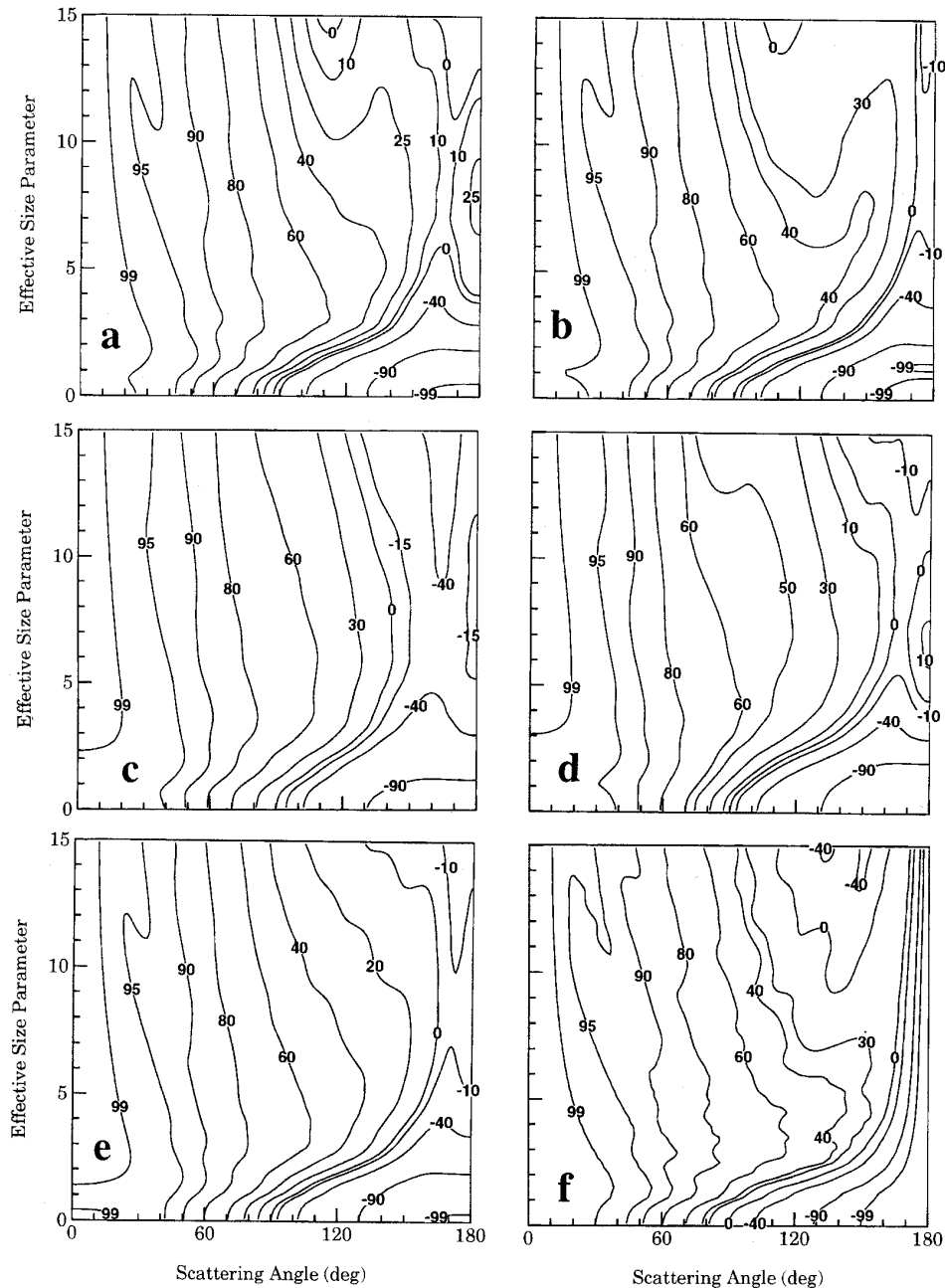


Fig. 11. Contour plots of the ratio $F_{44}/F_{11} \times 100\%$ as a function of scattering angle Θ and effective size parameter x_{eff} for surface-equivalent polydispersions of (a) prolate and (b) oblate spheroids with the aspect ratio $\epsilon = 1.5$, (c) prolate and (d) oblate spheroids with the aspect ratio $\epsilon = 2.2$, (e) an equiprobable mixture of 24 spheroidal shapes, and (f) spheres.

down to $x_{\text{eff}} = 0$, and regions 4 and 5 extend down to $x_{\text{eff}} = 2-3$. Below $x_{\text{eff}} = 2$, spherical-nonspherical differences are small, except for a region at $\Theta \geq 100^\circ$ for $x_{\text{eff}} \sim 1$, where nonspherical particles are stronger scatterers than spheres by as much as several tens of percent.

All the five regions can be clearly seen in calculations for the equiprobable shape mixture [Fig. 8(e)]. As is the case for the integral photometric quantities,

the phase function of oblate spheroids with the aspect ratio $\epsilon = 1.7$ most closely resembles that of the shape mixture, the percent differences being less than $\pm 30\%$ in most cases. These differences are relatively larger because the dependence of the phase function on the particle aspect ratio is not as monotonic as in the case of the integral photometric quantities and is somewhat different for prolate and oblate spheroids of the same aspect ratio.

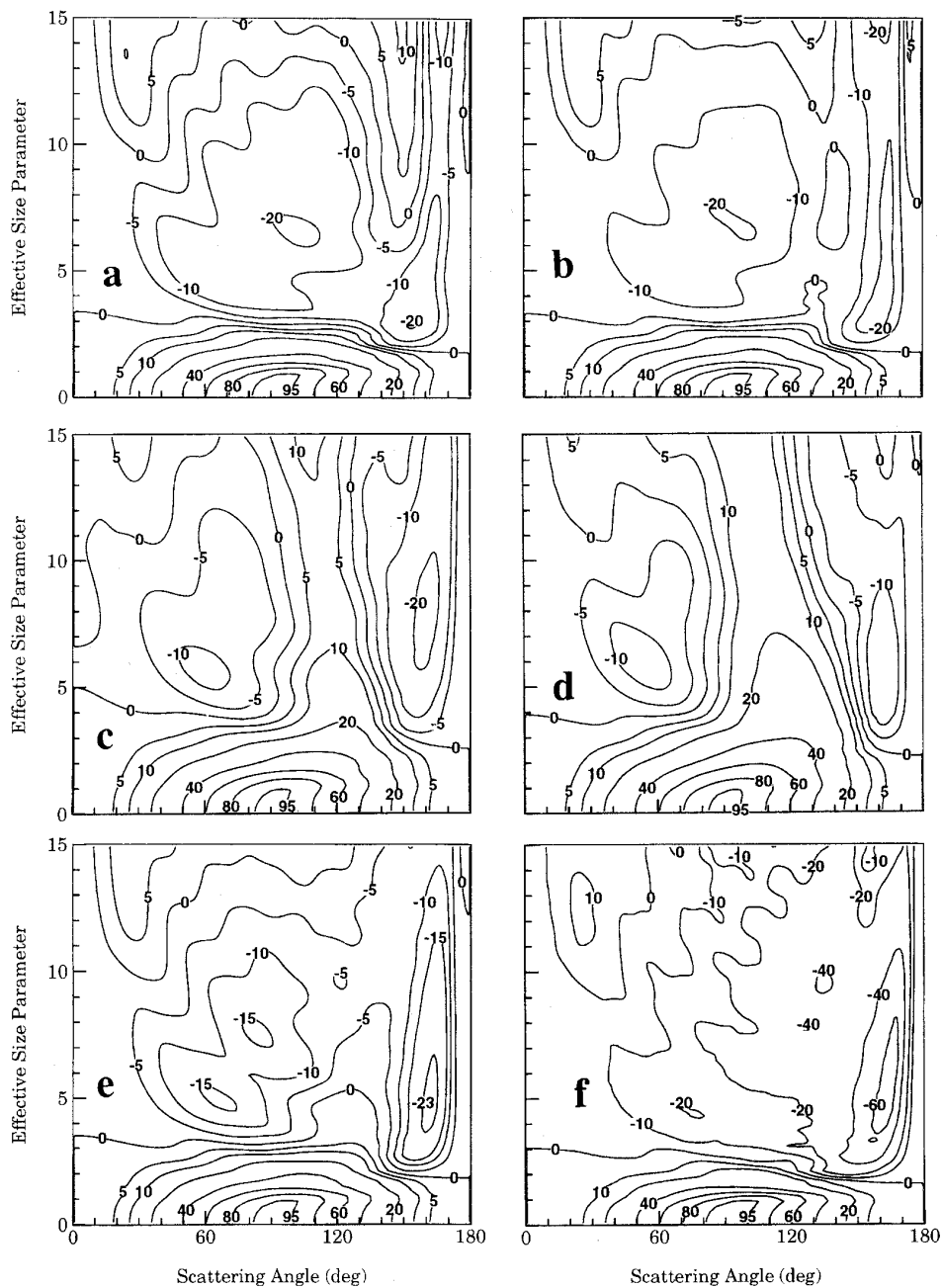


Fig. 12. Contour plots of linear polarization $-F_{12}/F_{11} \times 100\%$ as a function of scattering angle Θ and effective size parameter x_{eff} for surface-equivalent polydispersions of (a) prolate and (b) oblate spheroids with the aspect ratio $\epsilon = 1.5$, (c) prolate and (d) oblate spheroids with the aspect ratio $\epsilon = 2.2$, (e) an equiprobable mixture of 24 spheroidal shapes, and (f) spheres.

C. F_{22}/F_{11}

Although for spheres the ratio F_{22}/F_{11} is identically equal to 1 [Eq. (22)], for spheroids it can substantially deviate from unity, especially at side- and backscattering angles ($\Theta > 70^\circ$ – 80°), as illustrated in Fig. 9, in which the angular dependence of F_{22}/F_{11} is rather different for prolate and oblate spheroids of the same aspect ratio. In particular, for prolate spheroids the ratio F_{22}/F_{11} is especially size and aspect ratio dependent.

Also, for prolate spheroids the smallest F_{22}/F_{11} values are concentrated at smaller scattering angles, and the minimum F_{22}/F_{11} values are smaller than for oblate spheroids. As a result, measurements of the angular behavior of F_{22}/F_{11} at $\Theta > 70$ – 80° in laboratory experiments or bidirectional remote-sensing observations may, potentially, be used to distinguish between prolate and oblate particles and to determine particle size and aspect ratio. On the other hand, at

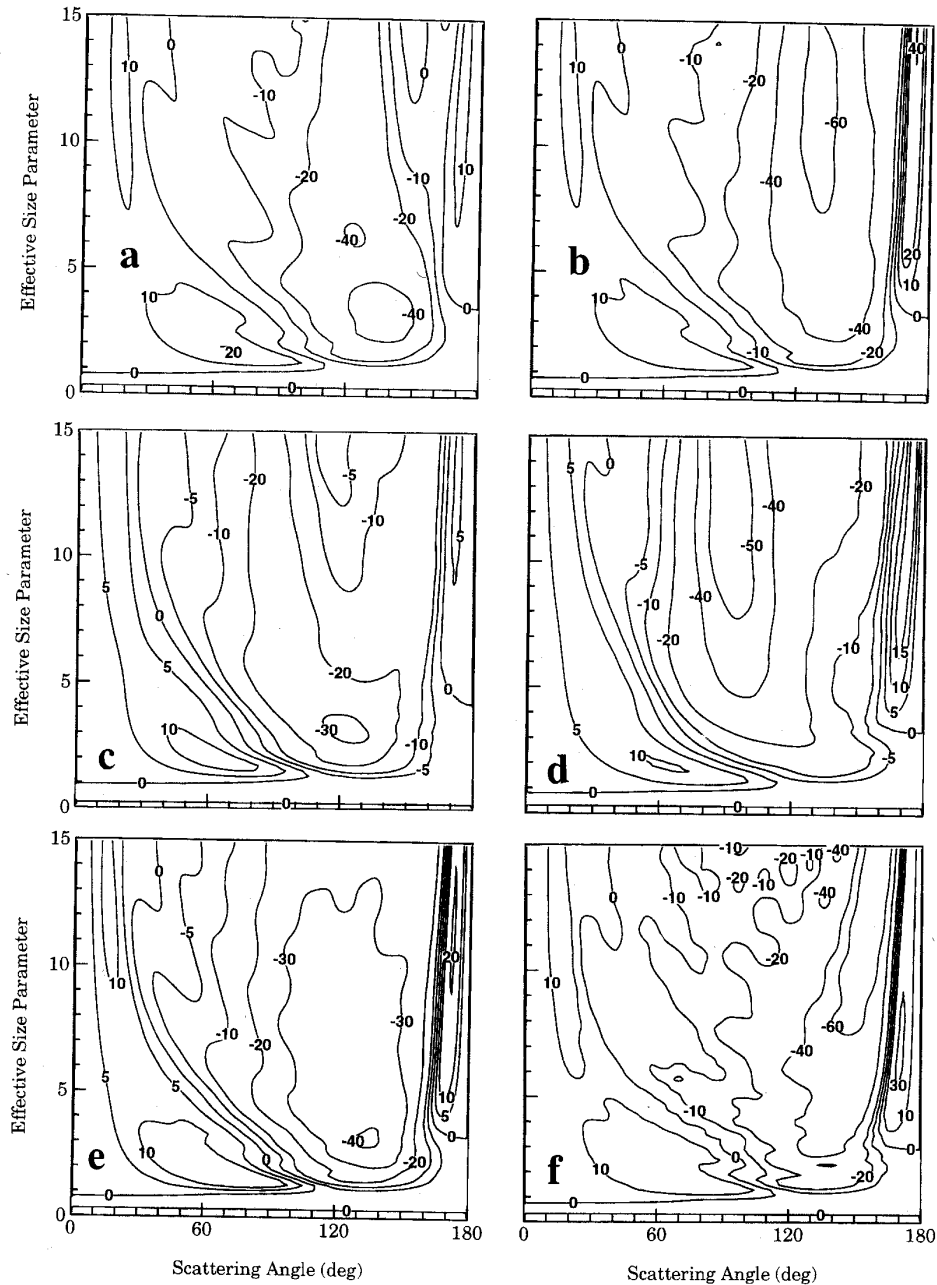


Fig. 13. Contour plots of the ratio $F_{34}/F_{11} \times 100\%$ as a function of scattering angle Θ and effective size parameter x_{off} for surface-equivalent polydispersions of (a) prolate and (b) oblate spheroids with the aspect ratio $\epsilon = 1.5$, (c) prolate and (d) oblate spheroids with the aspect ratio $\epsilon = 2.2$, (e) an equiprobable mixture of 24 spheroidal shapes, and (f) spheres.

scattering angles less than roughly 70° and in the region of Rayleigh scattering ($x_{\text{off}} \leq 1$), the ratio F_{22}/F_{11} is close to 1 and is practically insensitive to particle size and shape.

The ratio F_{22}/F_{11} for the equiprobable shape mixture [Fig. 9(e)] is closer to that for oblate spheroids than for prolate spheroids. This can be explained by the fact that F_{22}/F_{11} is strongly aspect ratio dependent for prolates and nearly aspect ratio independent

for oblates with aspect ratios larger than roughly 1.4. As a result, particular details specific for prolate spheroids with different aspect ratios are averaged out, and the shape-averaged pattern is dominated by nearly aspect-ratio-independent features of oblate scattering. We have found that the ratio F_{22}/F_{11} for the equiprobable shape mixture is best represented by the ratio F_{22}/F_{11} of oblate spheroids with the aspect ratio 1.9, percent differences being smaller

than $\pm 18\%$ in the whole range of scattering angles and effective size parameters.

D. F_{33}/F_{11} and F_{44}/F_{11}

Whereas for spherical particles $F_{33}/F_{11} \equiv F_{44}/F_{11}$, for spheroids these ratios may be substantially different (Figs. 10 and 11). In particular, our calculations show that unlike the ratio F_{33}/F_{11} , the ratio F_{44}/F_{11} may be positive at $\Theta = 180^\circ$. For most effective size parameters and scattering angles, the ratio F_{44}/F_{11} is larger than F_{33}/F_{11} . This conclusion is in agreement with laboratory measurements by Perry *et al.*²⁹ for NaCl particles and theoretical computations for randomly oriented monodisperse spheroids by Asano and Sato.²⁸ At side- and backscattering angles, these ratios are (strongly) size and shape dependent, thus being sensitive indicators of particle size and shape. In particular, these ratios are appreciably different for prolate and oblate spheroids of the same aspect ratio and, therefore, may be used to distinguish between prolate and oblate particles. The region of phase angles where the ratio F_{33}/F_{11} is negative is narrower for oblate spheroids than for prolate spheroids of the same aspect ratio.

For the equiprobable shape mixture [Figs. 10(e) and 11(e)], the ratios F_{33}/F_{11} and F_{44}/F_{11} are substantially different at phase angles larger than 90° . The ratio F_{44}/F_{11} is systematically larger than F_{33}/F_{11} , except for the region of forward and near-forward scattering, where the ratio F_{33}/F_{11} may be slightly larger. Because of the strong and complicated dependence of these ratios on particle shape, the shape-averaged patterns cannot be sufficiently accurately represented by those of a single effective spheroidal shape.

In accordance with the general inequality^{31,32}

$$|F_{33} - F_{44}| \leq F_{11} - F_{22}, \quad (25)$$

the difference between the ratios F_{33}/F_{11} and F_{44}/F_{11} is less than the deviation of the ratio F_{22}/F_{11} from unity. However, we have found from our calculations that the inequality of Eq. (25) is close to equality, especially for prolate spheroids (cf. Stammes⁶). Specifically, although for spheres the ratio

$$\Delta = \frac{F_{11} - F_{22} + F_{33} - F_{44}}{F_{11}} \times 100\% \quad (26)$$

is identically equal to zero, for spheroids this ratio may be nonzero but, in the whole range of effective size parameters and scattering angles, does not exceed 8.5% for prolate spheroids, 19% for oblate spheroids, and 6.8% for the shape mixture (see Table 2, which shows the maximum Δ value on the interval $x_{\text{eff}} \in [0, 15]$ for each of the spheroidal shapes and for the equiprobable shape mixture as well as the effective size parameter x_Δ and scattering angle Θ_Δ at which this maximum value is reached). At exactly

Table 2. Maximum Values of the Ratio Δ and Backscattering Depolarization Ratios δ_L and δ_C Along with Corresponding Values of the Effective Size Parameter and Scattering Angle for Prolate and Oblate Spheroids with Varying Aspect Ratios and the Equiprobable Shape Mixture

ϵ	$\Delta^{\text{max}} (\%)$	x_Δ	$\Theta_\Delta (\text{deg})$	δ_L^{max}	x_L	δ_C^{max}	x_C
Prolate spheroids							
1.1	1.30	11.6	24	0.270	15	0.740	15
1.2	2.00	12.8	44	0.475	15	1.807	15
1.3	3.53	13.8	110	0.515	10.8	2.119	10.8
1.4	4.67	12.4	98	0.502	9	2.014	9
1.5	5.91	12	91	0.467	8.4	1.751	8.4
1.6	6.76	12.8	96	0.438	7.2	1.561	7.2
1.7	5.67	12	101	0.403	7.2	1.348	7.2
1.8	5.85	12.6	166	0.369	7.2	1.170	7.2
1.9	6.79	12.6	165	0.341	7	1.035	7
2	7.81	10.6	162	0.316	6.2	0.922	6.2
2.1	8.48	10.6	161	0.297	7.8	0.844	7.8
2.2	8.36	10.4	161	0.285	8	0.798	8
Oblate spheroids							
1.1	1.10	15	172	0.143	15	0.335	15
1.2	3.20	13.6	171	0.220	15	0.564	15
1.3	5.18	8.2	169	0.245	14.4	0.650	14.4
1.4	7.44	6.4	167	0.278	9.8	0.772	9.8
1.5	9.64	5.8	165	0.310	9.2	0.900	9.2
1.6	11.5	5	163	0.335	7.6	1.009	7.6
1.7	12.9	5	162	0.353	7.8	1.092	7.8
1.8	13.9	4.6	160	0.362	7.6	1.136	7.6
1.9	14.6	3.4	150	0.369	7.4	1.168	7.4
2	15.9	4.2	139	0.373	7.2	1.191	7.2
2.1	17.6	3.4	131	0.379	7	1.222	7
2.2	19.0	3.4	130	0.387	7	1.264	7
Equiprobable shape mixture							
	6.73	7.6	159	0.319	7.8	0.938	7.8

the backscattering direction,

$$\Delta(180^\circ) = 0, \quad (27)$$

which is in agreement with the general equality³³

$$F_{44}(180^\circ) - F_{33}(180^\circ) = F_{11}(180^\circ) - F_{22}(180^\circ). \quad (28)$$

Because F_{11} is always larger than or equal to F_{22} , Eq. (28) also yields

$$F_{44}(180^\circ) \geq F_{33}(180^\circ). \quad (29)$$

Note that the results of Hu *et al.*³³ imply that, for rotationally symmetric particles, the following equality holds at exactly the forward-scattering direction:

$$F_{11}(0) - F_{22}(0) - F_{33}(0) + F_{44}(0) = 0. \quad (30)$$

We have verified this equality in extensive T -matrix computations for spheroids and Chebyshev particles and recommend that it may be used as a convenient test in checking the accuracy of numerical calculations.

E. Linear Polarization ($-F_{12}/F_{11}$)

Figure 12 demonstrates that outside the region of Rayleigh scattering and at scattering angles larger than roughly 60° , linear polarization is strongly as-

pect ratio dependent, spherical–nonspherical differences increasing with increasing particle asphericity and making the Mie theory inapplicable in calculations for nonspherical particles at side- and backscattering angles. However, polarization patterns for prolate and oblate spheroids of the same aspect ratio are similar, indicating that aspect ratio may be a relevant shape parameter for linear polarization of light scattered by convex bodies (cf. Refs. 13, 19, 28, and 34). In general, linear polarization becomes more neutral with increasing aspect ratio. The most remarkable polarization feature of nonspherical scattering is the bridge of positive polarization at scattering angles near 120° , which extends from the region of Rayleigh scattering and may be used to distinguish between spherical and nonspherical shapes.^{19,28} This bridge of positive polarization was first found by Perry *et al.*²⁹ in their laboratory measurements of light scattering by submicrometer- and micrometer-sized nearly cubical NaCl particles and then by Asano and Sato²⁸ in their theoretical computations for monodisperse randomly oriented spheroids. At small scattering angles ($\leq 60^\circ$), linear polarization depends rather weakly on particle shape. Therefore Mie scattering computations of linear polarization for equivalent spheres at forward- and near-forward-scattering angles can potentially be used for sizing nonspherical particles.

Strong and peculiar dependence of linear polarization on particle aspect ratio makes it rather difficult to select a single spheroidal shape reasonably accurately representing the shape-averaged pattern [Fig. 12(e)]. Our calculations show that of all the 24 spheroidal shapes, an oblate spheroid with the aspect ratio 1.4 is, apparently, the best effective shape. However, in the regions of nearly neutral polarization, even the sign of polarization may be different for the equiprobable shape mixture and this effective spheroid.

F. F_{34}/F_{11}

Figure 13 shows that in the region of Rayleigh scattering ($x_{\text{eff}} \leq 1$), the ratio F_{34}/F_{11} is equal or close to zero for all the particle shapes. For larger particles, whatever their shape is, F_{34}/F_{11} is positive at forward- and backscattering angles and negative at side-scattering angles. The backscattering positive branch is narrow, and the forward-scattering positive branch, being narrow at $x_{\text{eff}} = 1.5$, broadens with decreasing size parameter, extends up to $\Theta = 110^\circ$ at $x_{\text{eff}} = 1.5$, and has a local maximum at around $\Theta = 60^\circ$ and $x_{\text{eff}} = 2.5$. Thus the general pattern of the sign of the ratio F_{34}/F_{11} as a function of the scattering angle and the effective size parameter is basically the same for all the particle shapes. This conclusion is in full agreement with laboratory measurements for NaCl particles by Perry *et al.*²⁹ However, large magnitude variations of the ratio F_{34}/F_{11} with changing shape make it sensitive to the fact of particle nonsphericity and rather different for prolate and oblate spheroids of the same aspect ratio. In particu-

lar, the backscattering positive branch is much weaker for prolate than for oblate spheroids. The negative minimum of the ratio F_{34}/F_{11} weakens and moves toward smaller scattering angles as the aspect ratio increases. The minimum is deeper and is reached at much larger size parameters for oblate spheroids than for prolate spheroids of the same aspect ratio. In general, prolate–spherical differences are larger than oblate–spherical ones. Figure 13 also demonstrates that F_{34}/F_{11} is (strongly) size dependent. Therefore this ratio is, potentially, a sensitive indicator of both particle shape and size, especially at scattering angles larger than 60° . At scattering angles less than 60° , F_{34}/F_{11} is much less shape dependent, as first noticed by Perry *et al.*,²⁹ thus making the Mie theory applicable to sizing of nonspherical particles.

Because of the strong variability of F_{34}/F_{11} with particle size and shape, the shape-averaged pattern of this ratio is dissimilar to that of any of the individual spheroidal shapes. As in the case of the ratios F_{33}/F_{11} and F_{44}/F_{11} , this makes it practically impossible to select an effective spheroidal shape that represents the F_{34}/F_{11} pattern of the equiprobable shape mixture reasonably well.

G. Backscattering Depolarization Ratios

Two quantities frequently measured in lidar and radar observations are the linear, δ_L , and circular, δ_C , backscattering depolarization ratios.^{35–42} The first quantity refers to the case of linearly polarized incident light and is the ratio of the cross-polarized to copolarized components of the backscattered light. The second quantity is relevant to the case of circularly polarized incident radiation and is the ratio of the same-helicity to opposite-helicity components of the backscattered signal. In terms of the Stokes scattering matrix \mathbf{F} given by Eq. (5), the depolarization ratios can be expressed as

$$\delta_L = \frac{F_{11}(180^\circ) - F_{22}(180^\circ)}{F_{11}(180^\circ) + F_{22}(180^\circ)}, \quad (31)$$

$$\delta_C = \frac{F_{11}(180^\circ) + F_{44}(180^\circ)}{F_{11}(180^\circ) - F_{44}(180^\circ)}. \quad (32)$$

Because for spheres $\delta_L \equiv 0$ and $\delta_C \equiv 0$, the depolarization ratios are usually considered sensitive indicators of particle nonsphericity.⁴³

Table 2 shows maximum values of the depolarization ratios on the interval $x_{\text{eff}} \in [0, 15]$ for each of the spheroidal shapes and for the shape mixture. Also, the quantities x_L and x_C are effective size parameters at which these maximum values are found. Several interesting specific features are seen from Table 2. First, for both prolate and oblate spheroids, the depolarization ratios can substantially deviate from zero, reaching $\delta_L = 0.515$ and $\delta_C = 2.119$ for prolate spheroids and $\delta_L = 0.387$ and $\delta_C = 1.264$ for oblate spheroids. Second, prolate and oblate spheroids behave quite differently with increasing aspect ratio:

although the depolarization ratios for oblate spheroids increase monotonically, those for prolate spheroids have a sharp maximum at a relatively small aspect ratio $\epsilon = 1.3$. Thus, for oblate spheroids, the depolarization ratios are indicators of the degree of particle asphericity, whereas for prolate spheroids almost spherically shaped particles can produce much greater depolarization than highly aspherical scatterers. Third, for both prolate and oblate spheroids, $x_L \equiv x_C$ and the aspect-ratio dependence of the ratios δ_L and δ_C is fully correlated: δ_C increases where δ_L increases and decreases where δ_L decreases. Thus we may conclude that both the linear and circular backscattering depolarization ratios are produced by exactly the same scattering mechanism. Note that several mechanisms have been suggested to explain depolarization of the backscattered light by nonspherical particles (see, e.g., Ref. 28). However, it is still not clear enough whether any of the mechanisms can explain all the specific features seen from Table 2.

4. Concluding Remarks

In this paper we have described the results of an extensive study of light scattering by polydispersions of randomly oriented prolate and oblate spheroids. Our main interest has been in light scattering by polydisperse models of nonspherical particles because averaging over sizes provides more realistic modeling of natural ensembles of scattering particles and washes out the interference structure and ripple typical for monodisperse scattering patterns, thus enabling one to derive meaningful conclusions about the effects of particle nonsphericity on light scattering.

Following Hansen and Travis,¹⁶ we have shown that light-scattering properties of any physically plausible distribution of equivalent-sphere radii of nonspherical particles depend primarily on only two parameters, namely, the effective radius and effective variance of the distribution, the actual shape of the distribution having a minor influence. To minimize CPU-time consumption, we have adopted in this paper a computationally convenient power law size distribution. However, in accordance with the above-mentioned result, we expect that all our computations and conclusions are valid for any other distribution, e.g., gamma and log-normal distributions, having the same effective radius and effective variance.

To display the large volume of numerical data, we have relied on contour plots of the elements of the scattering matrix as functions of scattering angle and effective size parameter following the example of Hansen and Travis¹⁶ and Coffeen and Hansen.⁴⁴ This way of representing the results permits the economical display of the continuous sequence of calculations for the whole range of scattering angles and size parameters, thus illustrating the general pattern of light scattering, while nonetheless permitting values to be read off the contour plot with an accuracy still good enough for many practical purposes.

We have demonstrated on the basis of our rigorous

computations that polydisperse spherical–nonspherical differences in the angular distribution of the scattered intensity can be large. This result may have important consequences for remote sensing of tropospheric aerosols^{30,45,46} because a substantial fraction of aerosol particles are solid and, thus, have nonspherical shapes. As follows from our computations, even for such a modest aspect ratio as 1.5 the scattered intensity can be smaller or larger than that for equivalent spheres by as significant a factor as 2.5. Therefore we must conclude that if aerosol particles are even moderately aspherical, then the Mie theory should not be used to interpret results of photometric remote-sensing measurements.

Polydisperse nonspherical phase functions are rather flat at side-scattering angles, especially for larger aspect ratios, and show a modest backscattering peak, whereas phase functions for equivalent spheres demonstrate a wide and deep side-scattering minimum and a pronounced glory. As a result, spherical–nonspherical differences in scattered intensity are most significant at side- and backscattering angles. However, these differences are appreciable at near-forward-scattering angles as well, thus making reliable comparisons of experimentally measured nonspherical phase functions with theoretical computations for equivalent spheres difficult.

Unlike the phase function, spherical–nonspherical differences in polydisperse optical cross sections, single-scattering albedo, and asymmetry parameter of the phase function are much less pronounced. This suggests that the effects of particle shape may be less important for climate than for remote sensing.¹ However, the final conclusion should be made on the basis of accurate radiative transfer calculations for nonspherical versus spherical aerosols.⁴⁷ An important result of our calculations is that polydisperse nonspherical asymmetry factors may be larger than spherical factors in the region of effective size parameters from 3 to roughly 10–13, thus demonstrating the weakness of the semi-empirical approach²⁷ to nonspherical scattering.

All the elements of the polydisperse scattering matrix are complicated functions of particle shape and, for different nonspherical particles of equal size, may (substantially) differ in magnitude and even sign. At side- and backscattering angles, the ratio F_{22}/F_{11} is much more size and aspect ratio dependent for prolate spheroids than for oblate spheroids. Unlike spheres, for which $F_{33}/F_{11} \equiv F_{44}/F_{11}$, for spheroids the ratio F_{44}/F_{11} is usually larger than F_{33}/F_{11} , especially at side- and backscattering regions, and may even be positive at 180°. A common feature of nonspherical linear polarization is the bridge of positive polarization at 120° extending upward from the region of Rayleigh scattering. The general pattern of the sign of the ratio F_{34}/F_{11} as a function of the scattering angle and particle size is basically the same for all particle shapes and includes two positive branches at forward- and backscattering angles separated by a wide negative region. However, strong

variability of the magnitude of this ratio with particle shape makes it appreciably different for prolate and oblate spheroids. Because all the elements of the scattering matrix are (strongly) size and aspect ratio dependent, they are sensitive indicators of particle size and asphericity. Unlike the phase function and linear polarization, the ratios F_{22}/F_{11} , F_{33}/F_{11} , F_{44}/F_{11} , and F_{34}/F_{11} may be substantially different for prolate and oblate spheroids of the same aspect ratio and may be used to distinguish between prolate and oblate particles. Generally, all the elements of the polydisperse scattering matrix are (much) less shape dependent at scattering angles smaller than roughly 60° than at side- and backscattering angles. All our conclusions are in full agreement with laboratory measurements by Perry *et al.*²⁹ for nearly cubically shaped, micrometer- and submicrometer-sized NaCl particles, thus suggesting that spheroids can well represent light-scattering properties of convex particles.

The linear and circular backscattering depolarization ratios are produced by exactly the same scattering mechanism and, depending on particle shape and effective size parameter, can reach values as large as $\delta_L = 0.515$ and $\delta_C = 2.12$. However, the aspect-ratio dependence of the ratios for prolate and oblate spheroids is quite different and can be used to distinguish between prolate and oblate shapes. Surprisingly, for prolate spheroids both depolarization ratios have a sharp maximum at the relatively small, $\epsilon = 1.3$, aspect ratio and thus cannot be considered a measure of particle asphericity.

In most cases of practical interest, scattering particles are mixtures of different shapes. Unfortunately, the information about the distribution of particle shapes in natural ensembles is extremely limited. If a particle-shape distribution has a strong mode at a particular aspect ratio, then we can expect that light-scattering properties of such a narrow shape distribution are well represented by computations for a single particle shape. Another extreme case is a flat, aspect-ratio-independent shape distribution. To model such a case, we have computed light scattering by the simplest, equiprobable distribution of the 24 prolate and oblate spheroidal shapes with aspect ratios from 1.1 to 2.2. Not surprisingly, we have found that in the whole range of effective size parameters, the optical cross sections, single-scattering albedo, and asymmetry parameter of the phase function for the equiprobable shape mixture are rather accurately represented by those of a single, effective spheroid (an oblate spheroid with the aspect ratio 1.7). This result can be explained by the fact that these integral photometric quantities are relatively simple functions of particle size parameter and shape. On the other hand, the elements of the scattering matrix for the equiprobable shape mixture may differ substantially from those of any of the individual spheroids, thus making it difficult, if at all possible, to select a single spheroidal shape adequately representing this type of shape mixture.

We have found that the phase function and the ratio F_{22}/F_{11} for the equiprobable shape mixture are relatively close to those for oblate spheroids with aspect ratios 1.7 and 1.9, respectively, and the shape-averaged linear polarization qualitatively resembles that for oblate spheroids with the aspect ratio 1.4. As to the remaining elements of the scattering matrix, it is practically impossible to select a single effective spheroidal shape to represent the equiprobable shape mixture. Even the fact that the shape-averaged phase function, the ratio F_{22}/F_{11} , and the linear polarization are represented by different single aspect ratios suggests that the concept of an effective spheroidal shape hardly works in the case of the equiprobable shape distribution. This can be explained by the fact that the elements of the scattering matrix are (much) more complicated functions of particle size parameter and shape than the integral photometric quantities and may be substantially different for prolate and oblate spheroids of the same aspect ratio.

We must allow, following Wiscombe,⁴⁸ that spheroidal particles are special in one way: they are convex bodies. As was pointed out in Refs. 1–3 and 19, partial concavity of particle shape may have a pronounced effect on light scattering. Because many natural aerosol particles may have partially concave shapes, a survey of polydisperse concave nonspherical scattering similar to this survey of polydisperse convex spheroidal scattering would be useful. Unfortunately, straightforward *T*-matrix computations for partially concave Chebyshev particles become very slow for deformation parameters greater than 0.1–0.15.²⁶ Alternative methods for calculating nonspherical scattering such as the discrete dipole approximation⁴⁹ and the volume integral equation formulation⁵⁰ are, in principle, applicable to concave particles. However, they are much slower than the *T*-matrix method^{7,19} and may be practical only for relatively small size parameters. Thus it does not seem realistic to attempt a theoretical survey of polydisperse concave scattering comparable in scope to the present study at this time. Perhaps the most simple and efficient way to study polydisperse concave scattering extensively is to use one of the modifications of the *T*-matrix method^{51–53} in combination with the analytic averaging procedure⁹ to compute light scattering by polydisperse, randomly oriented bispheres. Of course, controlled laboratory experiments can also provide valuable information about the light-scattering properties of concave particles.^{50,54,55}

Finally, we note that the principal output of our computational method in the form of expansion coefficients (see equations 4–9 of Ref. 13) can be directly used in numerical solutions of the radiative transfer equation.⁵⁶ As was demonstrated by Hansen and Travis,¹⁶ multiple scattering does not necessarily dilute particular features of the single-scattering matrix, e.g., especially those of the single-scattering polarization. Therefore the Stokes param-

eters of multiply scattered light can be rather sensitive to particle nonsphericity.^{57,58}

We are grateful to J. E. Hansen, A. A. Lacis, B. E. Carlson, N. V. Voshchinnikov, and M. Sato for many valuable discussions and J. W. Hovenier, J. F. de Haan, F. Kuik, E. G. Yanovitskij, M. Wendisch, and an anonymous reviewer for their comments on an earlier version of the paper. This work was supported in part by the Earth Observing System Project managed by the NASA Goddard Space Flight Center in providing for the Earth Observing Scanning Polarimeter instrument analysis and algorithm development and by the NASA Office of Mission to Planet Earth.

References and Notes

1. A. Mugnai and W. J. Wiscombe, "Scattering from nonspherical Chebyshev particles. 1: Cross sections, single-scattering albedo, asymmetry factor, and backscattered fraction," *Appl. Opt.* **25**, 1235–1244 (1986).
2. W. J. Wiscombe and A. Mugnai, "Scattering from nonspherical Chebyshev particles. 2: Means of angular scattering patterns," *Appl. Opt.* **27**, 2405–2421 (1988).
3. A. Mugnai and W. J. Wiscombe, "Scattering from nonspherical Chebyshev particles. 3: Variability in angular scattering patterns," *Appl. Opt.* **28**, 3061–3073 (1989).
4. S. C. Hill, A. C. Hill, and P. W. Barber, "Light scattering by size/shape distributions of soil particles and spheroids," *Appl. Opt.* **23**, 1025–1031 (1984).
5. J. F. de Haan, "Effects of aerosols on the brightness and polarization of cloudless planetary atmospheres," Ph.D. dissertation (Free University, Amsterdam, 1987).
6. P. Stammes, "Light scattering properties of aerosols and the radiation inside a planetary atmosphere," Ph.D. dissertation (Free University, Amsterdam, 1989).
7. F. Kuik, "Single scattering of light by ensembles of particles with various shapes," Ph.D. dissertation (Free University, Amsterdam, 1992).
8. F. Kuik, J. F. de Haan, and J. W. Hovenier, "Benchmark results for single scattering by spheroids," *J. Quant. Spectrosc. Radiat. Transfer* **47**, 477–489 (1992).
9. M. I. Mishchenko, "Light scattering by randomly oriented axially symmetric particles," *J. Opt. Soc. Am. A* **8**, 871–882 (1991); **9**, 497(E) (1992).
10. P. C. Waterman, "Symmetry, unitarity, and geometry in electromagnetic scattering," *Phys. Rev. D* **3**, 825–839 (1971); S. Ström, "On the integral equations for electromagnetic scattering," *Am. J. Phys.* **43**, 1060–1069 (1975); P. Barber and C. Yeh, "Scattering of electromagnetic waves by arbitrarily shaped dielectric bodies," *Appl. Opt.* **14**, 2864–2872 (1975).
11. V. K. Varadan and V. V. Varadan, eds., *Acoustic, Electromagnetic and Elastic Wave Scattering—Focus on the T-Matrix Approach* (Pergamon, New York, 1980).
12. L. Tsang, J. A. Kong, and R. T. Shin, *Theory of Microwave Remote Sensing* (Wiley, New York, 1985).
13. M. I. Mishchenko, "Light scattering by size/shape distributions of randomly oriented axially symmetric particles of size comparable to a wavelength," *Appl. Opt.* **32**, 4652–4666 (1993).
14. M. I. Mishchenko and L. D. Travis, "T-matrix computations of light scattering by large spheroidal particles," *Opt. Commun.* **109**, 16–21 (1994).
15. H. C. van de Hulst, *Light Scattering by Small Particles* (Wiley, New York, 1957).
16. J. E. Hansen and L. D. Travis, "Light scattering in planetary atmospheres," *Space Sci. Rev.* **16**, 527–610 (1974).
17. C. F. Bohren and D. R. Huffman, *Absorption and Scattering of Light by Small Particles* (Wiley, New York, 1983).
18. M. Hofer and O. Glatter, "Mueller matrix calculations for randomly oriented rotationally symmetric objects with low contrast," *Appl. Opt.* **28**, 2389–2400 (1989).
19. M. I. Mishchenko and L. D. Travis, "Light scattering by polydisperse rotationally symmetric nonspherical particles: linear polarization," *J. Quant. Spectrosc. Radiat. Transfer* **51**, 759–778 (1994).
20. F. Kuik, J. F. de Haan, and J. W. Hovenier, "Single scattering of light by circular cylinders," *Appl. Opt.* **33**, 4906–4918 (1994).
21. M. I. Mishchenko and L. D. Travis, "Light scattering by size/shape distributions of nonspherical particles of size comparable to a wavelength," in *Atmospheric Propagation and Remote Sensing II*, A. Kohnle and W. B. Miller, eds., Proc. Soc. Photo-Opt. Instrum. Eng. **1968**, 118–129 (1993).
22. V. Vouk, "Projected area of convex bodies," *Nature (London)* **162**, 330–331 (1948).
23. J. E. Hansen and J. W. Hovenier, "Interpretation of the polarization of Venus," *J. Atmos. Sci.* **31**, 1137–1160 (1974); M. I. Mishchenko, "Physical properties of the upper tropospheric aerosols in the equatorial region of Jupiter," *Icarus* **84**, 296–304 (1990).
24. A. Lacis, J. Hansen, and M. Sato, "Climate forcing by stratospheric aerosols," *Geophys. Res. Lett.* **19**, 1607–1610 (1992).
25. G. A. d'Almeida, P. Koepke, and E. P. Shettle, *Atmospheric Aerosols* (Deepak, Hampton, Va., 1991).
26. W. J. Wiscombe and A. Mugnai, "Single scattering from nonspherical Chebyshev particles: a compendium of calculations," NASA Ref. Publ. 1157 (Goddard Space Flight Center, NASA, Greenbelt, Md., 1986).
27. J. B. Pollack and J. N. Cuzzi, "Scattering by nonspherical particles of size comparable to a wavelength: a new semi-empirical theory and its application to tropospheric aerosols," *J. Atmos. Sci.* **37**, 868–881 (1980).
28. S. Asano and M. Sato, "Light scattering by randomly oriented spheroidal particles," *Appl. Opt.* **19**, 962–974 (1980).
29. R. J. Perry, A. J. Hunt, and D. R. Huffman, "Experimental determinations of Mueller scattering matrices for nonspherical particles," *Appl. Opt.* **17**, 2700–2710 (1978).
30. P. Koepke and M. Hess, "Scattering functions of tropospheric aerosols: the effects of nonspherical particles," *Appl. Opt.* **27**, 2422–2430 (1988).
31. E. S. Fry and G. W. Kattawar, "Relationships between elements of the Stokes matrix," *Appl. Opt.* **20**, 2811–2814 (1981).
32. J. W. Hovenier, H. C. van de Hulst, and C. V. M. van der Mee, "Conditions for the elements of the scattering matrix," *Astron. Astrophys.* **157**, 301–310 (1986).
33. C.-R. Hu, G. W. Kattawar, M. E. Parkin, and P. Herb, "Symmetry theorems on the forward and backward scattering Mueller matrices for light scattering from a nonspherical dielectric scatterer," *Appl. Opt.* **26**, 4159–4173 (1987).
34. D. W. Schuerman, R. T. Wang, B. Å. S. Gustafson, and R. W. Schaefer, "Systematic studies of light scattering. 1: Particle shape," *Appl. Opt.* **20**, 4039–4050 (1981).
35. K.-N. Liou and H. Lahore, "Laser sensing of cloud composition: a backscatter depolarization technique," *J. Appl. Meteorol.* **13**, 257–263 (1974).
36. D. W. Cooper, J. W. Davis, and R. L. Byers, "Measurements of depolarization by dry and humidified salt aerosols using a lidar analogue," *Aerosol Sci.* **5**, 117–123 (1974).
37. T. Oguchi, "Electromagnetic wave propagation and scattering in rain and other hydrometeors," *Proc. IEEE* **71**, 1029–1078 (1983).
38. K. Sassen, "The polarization lidar technique for cloud research: a review and current assessment," *Bull. Am. Meteorol. Soc.* **72**, 1848–1866 (1991).

39. S. Y. Matrosov, "Theoretical study of radar polarization parameters obtained from cirrus clouds," *J. Atmos. Sci.* **48**, 1062-1070 (1991).
40. P. H. Herzegh and A. R. Jameson, "Observing precipitation through dual-polarization radar measurements," *Bull. Am. Meteorol. Soc.* **73**, 1365-1374 (1992).
41. W. L. Eberhard, "Ice-cloud depolarization of backscatter for CO₂ and other infrared lidars," *Appl. Opt.* **31**, 6485-6490 (1992).
42. S. J. Ostro, G. H. Pettengill, and D. B. Campbell, "Radar observations of Saturn's rings at intermediate tilt angles," *Icarus* **41**, 381-388 (1980); S. J. Ostro, G. H. Pettengill, D. B. Campbell, and R. M. Goldstein, "Delay-Doppler radar observations of Saturn's rings," *Icarus* **49**, 367-381 (1982).
43. Note, however, that multiple scattering can also produce significant depolarization of backscattered light, even for spherical particles [e.g., M. I. Mishchenko, "Polarization characteristics of the coherent backscatter opposition effect," *Earth Moon Planets* **58**, 127-144 (1992)]. Therefore, in analyzing observational or laboratory data, one should be careful in assigning the origin of nonzero backscattering depolarization ratios solely to particle nonsphericity.
44. D. L. Coffeen and J. E. Hansen, "Polarization studies of planetary atmospheres," in *Planets, Stars and Nebulae Studied with Photopolarimetry*, T. Gehrels, ed. (U. Arizona Press, Tucson, Ariz., 1974), pp. 518-592.
45. T. Nakajima, M. Tanaka, M. Yamano, M. Shiobara, K. Arai, and Y. Nakanishi, "Aerosol optical characteristics in the yellow sand events observed in May, 1982 at Nagasaki: Part II. Models," *J. Meteorol. Soc. Jpn.* **67**, 279-291 (1989).
46. Y. J. Kaufman, "Aerosol optical thickness and atmospheric path radiance," *J. Geophys. Res.* **98**, 2677-2692 (1993).
47. M. I. Mishchenko, B. E. Carlson, and A. A. Lacis, "Radiative properties of nonspherical aerosols," in *Proceedings of the Eighth Conference on Atmospheric Radiation* (American Meteorological Society, Boston, Mass., 1994), pp. 307-309.
48. W. Wiscombe, "Atmospheric radiation: 1975-1983," *Rev. Geophys. Space Phys.* **21**, 997-1021 (1983).
49. J. J. Goodman, B. T. Draine, and P. J. Flatau, "Application of fast-Fourier-transform techniques to the discrete-dipole approximation," *Opt. Lett.* **16**, 1198-1200 (1991).
50. J. I. Hage, J. M. Greenberg, and R. T. Wang, "Scattering from arbitrarily shaped particles: theory and experiment," *Appl. Opt.* **30**, 1141-1152 (1991).
51. B. Peterson and S. Ström, "T matrix for electromagnetic scattering from an arbitrary number of scatterers and representations of E(3)*," *Phys. Rev. D* **8**, 3661-3678 (1973).
52. K. A. Fuller and G. W. Kattawar, "Consummation solution to the problem of classical electromagnetic scattering by an ensemble of spheres. 1: Linear chains," *Opt. Lett.* **13**, 90-92 (1988).
53. D. W. Mackowski, "Analysis of radiative scattering for multiple sphere configurations," *Proc. R. Soc. London Ser. A* **433**, 599-614 (1991).
54. R. H. Zerull, "Scattering measurements of dielectric and absorbing nonspherical particles," *Beitr. Phys. Atmos.* **49**, 168-188 (1976).
55. R. H. Zerull, B. Å. S. Gustafson, K. Schulz, and E. Thiele-Corbach, "Scattering by aggregates with and without an absorbing mantle: microwave and analog experiments," *Appl. Opt.* **32**, 4088-4100 (1993).
56. H. Domke, "The expansion of scattering matrices for an isotropic medium in generalized spherical functions," *Astrophys. Space Sci.* **29**, 379-386 (1974); J. W. Hovenier and C. V. M. van der Mee, "Fundamental relationships relevant to the transfer of polarized light in a scattering atmosphere," *Astron. Astrophys.* **128**, 1-16 (1983); M. I. Mishchenko, "Reflection of polarized light by plane-parallel slabs containing randomly-oriented, nonspherical particles," *J. Quant. Spectrosc. Radiat. Transfer* **46**, 171-181 (1991).
57. M. I. Mishchenko, "Enhanced backscattering of polarized light from discrete random media: calculations in exactly the backscattering direction," *J. Opt. Soc. Am. A* **9**, 978-982 (1992).
58. W. M. F. Wauben, J. F. de Haan, and J. W. Hovenier, "Influence of particle shape on the polarized radiation in planetary atmospheres," *J. Quant. Spectrosc. Radiat. Transfer* **50**, 237-246 (1993).

